Theoretical analysis of the influence of forced and inherent temperature fluctuations in an adiabatic chromatographic column

Shamsul Qamar[a,b,*], Fouzia A. Sattar[b], Iqra Batool[b], Andreas Seidel-Morgenstern[a]

[a] *Max Planck Institute for Dynamics of Complex Technical Systems Magdeburg, Germany*
[b] *Department of Mathematics, COMSATS Institute of Information Technology, Islamabad, Pakistan*

Abstract

A linearized non-isothermal equilibrium dispersive model (EDM) of liquid chromatography is investigated to quantify unavoidable thermal effects in adiabatic chromatographic columns. The considered model contains convection-diffusion partial differential equations (PDEs) for mass and energy balances in the mobile phase coupled with an algebraic equation for adsorption isotherm. The solution process successively employ Laplace transformation and linear transformation steps to uncouple the governing set of coupled differential equations. The resulting uncoupled systems of ordinary differential equations are solved using an elementary solution technique. The solutions are very useful to understand the speeds and shapes of concentration and thermal fronts in chromatographic columns. The moment generating property of the Laplace domain solutions is utilized to derive analytical temporal moments of the concentration and temperature profiles. These moments are seen as useful to estimate unknown model parameters from measured profiles. For illustration several case studies of practical interest are provided. To evaluate the range of applicability of analytical solutions, selected results are compared with numerical results applying a

*Corresponding author. Tel: +49-391-6110454; fax: +49-391-6110500
Email addresses: qamar@mpi-magdeburg.mpg.de (Shamsul Qamar)

high resolution finite volume scheme considering nonlinear isotherms.

Key words: Non-isothermal chromatography, linearized isotherm, analytical solutions, moment analysis, numerical solutions.

---

1. Introduction:

Chromatography is one of the most versatile separation techniques used for identification and purification of multi-component mixtures in many industries. It has a wide range industrial applications either as a preparative or analytical method. This technology is highly effective for the separation of complex mixtures and very similar target molecules at reasonable production and high purity levels, for instance to isolate enantiomers and to purify proteins, see Ruthven (1984); Guiochon (2002); Guiochon and Lin (2003); Guiochon et al. (2006).

Separation of mixture components through liquid chromatography is based on their different distribution between two non-miscible phases. The first one is a stationary solid phase which is fixed in the column. The second one is a mobile liquid phase streaming through the chromatographic system. Firstly, the liquid mixture (mobile phase) is fed into a column containing a stationary phase. The stationary phase adsorbs the mixture components in varying degrees. During the migration of mixture components through the column, composition fronts develop and propagate governed by the adsorption isotherm providing a characteristics retention behavior of the species involved. Separated peaks of desired purity can be collected periodically at the outlet of the column. Being an exothermic process, adsorption is always accompanied by heat transfer, which in certain situations

becomes very important.

Thermal effects are usually neglected in the liquid chromatography by assuming that the effect of heats of adsorption is negligible. For that reason, adsorption chromatography processes have often been assumed isothermal. The first analysis of thermal effects in a pulse chromatography experiment has been done by Cerro and Smith (1969). In that article, heat effects were analyzed by studying a deviation from linear chromatography through injection pulse size and concentration variations. In order to answer the question of whether the linearity of such systems is a sufficient condition to insure the absence of thermal effects, Haynes (1969) made a study based on temporal moment analysis. Zhong and Meunier (1994) have studied the interference for non-isothermal non-equilibrium perturbation chromatography by means of temporal moment analysis. They derived analytical expressions of the first and second chromatographic moments. There are few more contributions considering non-isothermal conditions in packed fixed-beds, see e.g. Sainio (2005, 2007, 2011); Tien (2011); Javeed et al. (2012). On the other hand, thermal effects have been widely discussed in the case of gas chromatography using solid packings, see e.g. Kruglov (1994); Yongsunthon (1999); Xiu (2002); Glockler (2006); Eigenberger (2007).

In high-pressure liquid chromatography, viscous heat generated by the friction of the eluent flowing through the packed-bed can be substantial and may cause a significant degrees rise in temperature along the column, see Gritti et al. (2016). Under steady state temperature regime, this heat generates radial temperature gradients that may cause serious losses of column efficiency, can significantly affect the solvent viscosity, and may overcome the effect of the adsorption heat. Thus, proper precautions are necessary to minimize heat

losses through the column wall. For more details about this phenomenon, which is not further considered below, see the article by Gritti et al. (2016) and references therein.

Different mathematical models are available in the literature for studying chromatographic separations at the analytical and preparative scales. The most important to mention are the general rate model (GRM), the linear driving force model, the lumped kinetic model (LKM), the equilibrium dispersive model (EDM), and the ideal model, see Ruthven (1984); Guiochon (2002); Guiochon and Lin (2003); Guiochon et al. (2006). Each model has its own level of complexity to describe the process. In this work, the non-isothermal EDM is analytically and numerically investigated. The EDM assumes that mass transfer is of infinite rate whereas the LKM incorporates the rate of variation of the local concentration of solute in the stationary phase and local deviation from equilibrium concentrations. The GRM accounts for axial dispersion and all the mass transfer resistances. The current single-component non-isothermal EDM consist of two convection-diffusion partial differential equations with dominant convective terms and coupled with an algebraic equation for isotherm.

The aim of this article is to quantify temperature gradients that occur in liquid chromatography. The joint occurrence of concentration and thermal fronts is illustrated and key parameters influencing the temperature gradients are identified. For this purpose, a linearized non-isothermal EDM is considered. The analytical solutions for concentration and energy are derived by means of Laplace transformation, see Genuchten (1981); Rice (1995); Javeed et al. (2013). The moment generating property of the Laplace domain solutions is utilized to get partly new analytical expressions for the temporal moments. The relevance

and importance of matching theoretically and experimentally determined moments for efficient parameter estimation is known since a long time. Moment analysis approach has been comprehensively discussed in the literature, see Kubin (1964, 1965); Kucera (1965); Schneider and Smith (1968); Suzuki (1973); Wolff et al. (1979, 1980); Ruthven (1984); Lenhoff (1987); Miyabe et al. (2000, 2003, 2007, 2009); Guiochon et al. (2006); Javeed et al. (2013); Qamar and Seidel-Morgenstern (2016). Moments analysis is standard in the chromatographic community related to analyzing the second moments or the heights equivalent to a theoretical plate (HETP) as a function of flow rate in order to evaluate column efficiencies (Guiochon et al. (2006)). No systematic use is made of moments of temperature responses.

For validation of our linear assumptions, a high resolution finite volume scheme (HR-FVS) is applied to solve the model for nonlinear isotherm, see Javeed et al. (2011, 2012). Several case studies are carried out to analyze the current non-isothermal chromatographic process. In the present research several aspects are addressed that have not been treated in this detail up to now for the considered non-isothermal EDM model. The Laplace transformation and eigne-decomposition techniques are applied to derive analytical solutions of the model equations. The temperature effects within the column are deeply discussed and analyzed. To further analyze the process, the first four temporal moments are derived for the concentration and temperature pulses. The effects of different kinetic and thermodynamic parameters are analyzed on the process. Finally, we have extended the considered HR-FVS to solve the non-isothermal model of chromatography for comparison and validation of our linear assumptions, see Javeed et al. (2011, 2012). Several test problems of practical

interest are considered.

The remaining parts of the paper are organized as follows. In Section 2, the considered non-isothermal EDM is briefly introduced. In Section 3, analytical solutions of the model are derived. In Section 4, analytical temporal moments are derived from the Laplace transformed solutions. Section 5 presents the results of various case studies. Finally, conclusions are drawn in Section 6.

2. The non-isothermal equilibrium dispersive model

Consider the flow of a single-solute along with an inert carrier through a chromatographic column packed with spherical adsorbent particles. A small change in the concentration is performed by injecting a pulse of concentration into an initially equilibrated column. The following simplifying assumptions are used: (i) The column is fully initially equilibrated. (ii) The bed is homogeneous and radial concentration gradients in the column are neglected. (iii) The compressibility of the mobile phase is negligible, i.e. the fluid is incompressible. (iv) There is no interaction between the solvent (carrier) and the solid phase. (v) The packing material used in the stationary phase is made of porous spherical and uniform size particles. (vi) The equilibrium relationships are linearized. In general, adsorption equilibrium relationships are not linear, however, the linearization is realistic for small sample changes or perturbations, and can give simple characteristic results. (vii) The influence of temperature on the physical properties as viscosity, density, heat capacity, and transport coefficients as axial dispersion and axial heat conductivity can be neglected. (viii) The axial dispersion coefficient and the axial heat conductivity coefficient are assumed

independent of flow rate.

The equilibrium-dispersive model (EDM) assumes that the mass transfer kinetics are of infinite rate. All contributions due to non-equilibrium and axial dispersion effects are aggregated into the corresponding apparent dispersion coefficient D_z. The classical mass balance equation of the single-component EDM for a fixed-bed chromatographic column is expressed as

$$\frac{\partial c}{\partial t} + u\frac{\partial c}{\partial z} = D_z\frac{\partial^2 c}{\partial z^2} - F\frac{\partial q^*}{\partial t}\,. \tag{1}$$

If the enthalpy of mixing and friction effects are neglected, the energy balance for a differential volume element in an adiabatic chromatographic column comes out to be

$$(\rho^L c_p^L + F\rho^S c_p^S)\frac{\partial T}{\partial t} + u\rho^L c_p^L\frac{\partial T}{\partial z} = \lambda_z\frac{\partial^2 T}{\partial z^2} + F(-\Delta H_A)\frac{\partial q^*}{\partial t}\,. \tag{2}$$

In the above equations, c and q^* denote the concentrations of solute in the mobile and adsorbed phases, respectively. Further, T represents the temperature, $F = (1-\epsilon)/\epsilon$ denotes the phase ratio in term of the external porosity ϵ, u is the interstitial velocity, D_z represents the axial dispersion coefficient, λ_z is the axial heat conductivity, ΔH_A denotes the enthalpy of adsorption, ρ represents the density per unit volume, c_p is the heat capacity, the superscripts L and S stands for liquid and solid phases, while t and x represent the time and axial coordinates of the column.

The amount of solute adsorbed depends on the temperature which can be described by a van't Hoff type relation using the enthalpy of adsorption. Thus, the phase equilibrium relation, assumed to be linear in concentration, is expressed as

$$q^*(c,T) = a_{\text{ref}} e^{\left(\frac{-\Delta H_{\text{A}}}{R_g}\left(\frac{1}{T}-\frac{1}{T_{\text{ref}}}\right)\right)} c. \tag{3}$$

Here, a_{ref} denotes the equilibrium (Henry's) constant at T_{ref} and R_g is the general gas constant. Let us define

$$c_1 = c, \quad q_1^* = q^*, \tag{4}$$

and apply the transformation

$$c_2 = T - T_{\text{ref}}, \quad q_2^* = \frac{\rho^S c_p^S}{\rho^L c_p^L}(T - T_{\text{ref}}) + \frac{\Delta H_A}{\rho^L c_p^L} q^*. \tag{5}$$

Here, T_{ref} denotes the reference temperature. Using Eqs. (4) and (5) in Eqs. (1) and (2), we get

$$\frac{\partial c_1}{\partial t} + u\frac{\partial c_1}{\partial z} = D_z \frac{\partial^2 c_1}{\partial z^2} - F\frac{\partial q_1^*}{\partial t}\,, \tag{6}$$

$$\frac{\partial c_2}{\partial t} + u\frac{\partial c_2}{\partial z} = \frac{\lambda_z}{\rho^L c_p^L}\frac{\partial^2 c_2}{\partial z^2} - F\frac{\partial q_2^*}{\partial t}\,. \tag{7}$$

To simply the notations and reduce the number of variables, the following dimensionless quantities are introduced:

$$Pe_m = \frac{Lu}{D_z}, \quad Pe_e = \frac{Lu\rho^L c_p^L}{\lambda_z}, \quad x = \frac{z}{L}, \quad \tau = \frac{ut}{L}. \tag{8}$$

Here, L is the column length, while Pe_m and Pe_e are the Peclet numbers for mass and energy, respectively. Using Eq. (8) in Eqs. (6) and (7), we obtain

$$\frac{\partial c_1}{\partial \tau} + \frac{\partial c_1}{\partial x} = \frac{1}{Pe_m}\frac{\partial^2 c_1}{\partial x^2} - F\frac{\partial q_1^*}{\partial \tau}, \tag{9}$$

$$\frac{\partial c_2}{\partial \tau} + \frac{\partial c_2}{\partial x} = \frac{1}{Pe_e}\frac{\partial^2 c_2}{\partial x^2} - F\frac{\partial q_2^*}{\partial \tau}. \tag{10}$$

The nonlinear equilibrium function between the mobile and stationary adsorbed phases in Eq. (3) can be linearized by taking Taylor's expansion up to the first order assuming small

changes in the concentration and temperature as follows

$$q_1^*(c,T) \approx q_1^*(c_{\text{ref}},T_{\text{ref}}) + \left.\frac{\partial q_1^*}{\partial T}\right|_{(c_{\text{ref}},T_{\text{ref}})} (T-T_{\text{ref}}) + \left.\frac{\partial q_1^*}{\partial c}\right|_{(c_{\text{ref}},T_{\text{ref}})} (c-c_{\text{ref}}), \tag{11}$$

where, c_{ref} denotes the reference concentration. On using Eqs. (3), (4) and (5) in Eq. (11), we obtain

$$q_1^*(c_1,c_2) = a_{\text{ref}} c_1 + \frac{\Delta H_A a_{\text{ref}} c_{\text{ref}}}{R_g T_{\text{ref}}^2} c_2. \tag{12}$$

After using Eq. (12) in Eq. (5), we get

$$q_2^*(c_1,c_2) = \frac{a_{\text{ref}}\Delta H_A}{\rho^L c_p^L} c_1 + \left(\frac{\rho^S c_p^S}{\rho^L c_p^L} + \frac{\Delta H_A^2 a_{\text{ref}} c_{\text{ref}}}{R_g T_{\text{ref}}^2 \rho^L c_p^L} \right) c_2. \tag{13}$$

Now using Eqs. (12) and (13) in Eqs. (9) and (10), we get

$$\frac{1}{Pe_m}\frac{\partial^2 c_1}{\partial x^2} - \frac{\partial c_1}{\partial x} = \beta_m \frac{\partial c_1}{\partial \tau} + \gamma \frac{\partial c_2}{\partial \tau}, \tag{14}$$

$$\frac{1}{Pe_e}\frac{\partial^2 c_2}{\partial x^2} - \frac{\partial c_2}{\partial x} = \alpha \frac{\partial c_1}{\partial \tau} + \beta_e \frac{\partial c_2}{\partial \tau}, \tag{15}$$

where

$$\beta_m = 1 + F a_{\text{ref}}, \quad \gamma = F\frac{\Delta H_A a_{\text{ref}} c_{\text{ref}}}{R_g T_{\text{ref}}^2}, \quad \alpha = F\frac{a_{\text{ref}}\Delta H_A}{\rho^L c_p^L}, \tag{16}$$

$$\beta_e = 1 + F\frac{\rho^S c_p^S}{\rho^L c_p^L} + F\frac{\Delta H_A^2 a_{\text{ref}} c_{\text{ref}}}{R_g T_{\text{ref}}^2 \rho^L c_p^L}. \tag{17}$$

Here, a_{ref} is a measure of the relative solid mass storage capacity. The second term on the right hand side of Eq. (17) denotes the corresponding relative solid heat storage capacity. The third (source) term is typically of minor relevance compared to the second (capacity) term.

In matrix notation, Eqs. (14) and (15) can be expressed as

$$\begin{bmatrix} \frac{1}{Pe_m} \\ \\ \frac{1}{Pe_e} \end{bmatrix} \frac{\partial^2}{\partial x^2} \begin{bmatrix} c_1 \\ \\ c_2 \end{bmatrix} - \frac{\partial}{\partial x} \begin{bmatrix} c_1 \\ \\ c_2 \end{bmatrix} = \begin{pmatrix} \beta_m & \gamma \\ \\ \alpha & \beta_e \end{pmatrix} \frac{\partial}{\partial \tau} \begin{bmatrix} c_1 \\ \\ c_2 \end{bmatrix}. \tag{18}$$

The initial conditions are defined as

$$c_1(x,0) = c_{1,\text{init}}, \quad c_2(x,0) = c_{2,\text{init}}\,, \tag{19}$$

where, $c_{2,\text{init}} = T_{\text{init}} - T_{\text{ref}}$. Here, $c_{1,\text{init}}$ and T_{init} are the initial concentration and temperature in the column. Moreover, the following simplified boundary conditions (BCs) are considered at the column inlet and outlet:

$$c_1(0,\tau) = \begin{cases} c_{1,\text{inj}}\,, & \text{if } 0 \le \tau \le \tau_{\text{inj}} \\ 0\,, & \tau > \tau_{\text{inj}} \end{cases}, \quad \frac{\partial c_1}{\partial x}(\infty,\tau) = 0\,, \tag{20a}$$

$$c_2(0,\tau) = \begin{cases} c_{2,\text{inj}}\,, & \text{if } 0 \le \tau \le \tau_{\text{inj}} \\ 0\,, & \tau > \tau_{\text{inj}} \end{cases}, \quad \frac{\partial c_2}{\partial x}(\infty,\tau) = 0\,, \tag{20b}$$

where

$$c_{2,\text{inj}} = (T_{\text{inj}} - T_{\text{ref}}), \quad \tau_{\text{inj}} = \frac{u t_{\text{inj}}}{L}\,. \tag{21}$$

Here, t_{inj} denotes the time of injection, $c_{1,\text{inj}}$ is the concentration of injected pulse, and T_{inj} is the temperature of injected sample. In liquid chromatography, the Peclet numbers of mass and energy are generally high (or axial dispersion and axial heat conductivity coefficients are small). Thus, the above simple Dirichlet boundary conditions are valid. However, for smaller Peclet numbers (or large axial dispersion and axial heat conductivity coefficients), the more accurate well-known Danckwerts boundary conditions are necessary that account for back-mixing.

3. Analytical solutions

The considered linearized non-isothermal EDM can conveniently be solved by means of the Laplace transformation. It is defined as

$$\bar{w}(x,s) = \int_0^\infty e^{-s\tau} w(x,\tau) d\tau, \qquad \tau \geq 0, \tag{22}$$

where, $w \in \{c_1, c_2\}$. By applying the above Laplace transformation on Eq. (18), we obtain

$$\begin{bmatrix} \frac{1}{Pe_m} \\ \\ \frac{1}{Pe_e} \end{bmatrix} \frac{\partial^2}{\partial x^2} \begin{bmatrix} \bar{c_1} \\ \\ \bar{c_2} \end{bmatrix} - \frac{\partial}{\partial x} \begin{bmatrix} \bar{c_1} \\ \\ \bar{c_2} \end{bmatrix} = \begin{pmatrix} \beta_m & \gamma \\ \\ \alpha & \beta_e \end{pmatrix} \begin{bmatrix} s\bar{c_1} - c_{1,\text{init}} \\ \\ s\bar{c_2} - c_{2,\text{init}} \end{bmatrix}. \tag{23}$$

As the above equations are coupled, our goal is to decouple this system by using the eigen-decomposition technique. The coefficient matrix B of the system is given as

$$B = \begin{pmatrix} \beta_m & \gamma \\ \\ \alpha & \beta_e \end{pmatrix}. \tag{24}$$

The above matrix is diagonalizable, as it has two distinct eigenvalues

$$\lambda_{1,2} = \frac{1}{2}\left[(\beta_m + \beta_e) \pm \text{sgn}(\beta_\text{m} - \beta_\text{e})\sqrt{(\beta_m - \beta_e)^2 + 4\alpha\gamma}\right], \tag{25}$$

where

$$\text{sgn}(\beta_m - \beta_e) = \begin{cases} 1, & \text{if } \beta_m \geq \beta_e, \\ \\ -1, & \text{if } \beta_m < \beta_e. \end{cases} \tag{26}$$

This sgn function helps in assigning the correct eigenvalues to concentration and temperature fronts. The corresponding two different eigenvectors are given as

$$x_1 = \begin{bmatrix} \lambda_1 - \beta_e \\ \\ \alpha \end{bmatrix}, \quad x_2 = \begin{bmatrix} \lambda_2 - \beta_e \\ \\ \alpha \end{bmatrix}. \tag{27}$$

Thus, the transformation matrix A, based on the above eigenvalues, can be expressed as

$$A = \begin{pmatrix} \lambda_1 - \beta_e & \lambda_2 - \beta_e \\ \alpha & \alpha \end{pmatrix}. \tag{28}$$

This matrix A can be effectively utilized in the following linear transformation

$$\begin{bmatrix} \bar{c_1} \\ \bar{c_2} \end{bmatrix} = \begin{pmatrix} \lambda_1 - \beta_e & \lambda_2 - \beta_e \\ \alpha & \alpha \end{pmatrix} \begin{bmatrix} \bar{b}_1 \\ \bar{b}_2 \end{bmatrix}, \tag{29}$$

or

$$\begin{aligned} \bar{c_1}(x,s) &= (\lambda_1 - \beta_e)\,\bar{b}_1(x,s) + (\lambda_2 - \beta_e)\,\bar{b}_2(x,s), \\ \bar{c_2}(x,s) &= \alpha\bar{b}_1(x,s) + \alpha\bar{b}_2(x,s). \end{aligned} \tag{30}$$

By applying the above linear transformation on Eq. (23), we get

$$\frac{1}{Pe_m}\frac{\partial^2\bar{b}_1}{\partial x^2} - \frac{\partial\bar{b}_1}{\partial x} - s\lambda_1\bar{b}_1 = -\lambda_1 b_{1,\text{init}}\,, \tag{31}$$

$$\frac{1}{Pe_e}\frac{\partial^2\bar{b}_2}{\partial x^2} - \frac{\partial\bar{b}_2}{\partial x} - s\lambda_2\bar{b}_2 = -\lambda_2 b_{2,\text{init}}\,, \tag{32}$$

where

$$b_{1,\text{init}} = \frac{c_{1,\text{init}}}{\lambda_1 - \lambda_2} + \frac{\beta_e - \lambda_2}{\alpha(\lambda_1 - \lambda_2)}c_{2,\text{init}}\,, \qquad b_{2,\text{init}} = -\frac{c_{1,\text{init}}}{\lambda_1 - \lambda_2} + \frac{\lambda_1 - \beta_e}{\alpha(\lambda_1 - \lambda_2)}c_{2\text{init}}\,. \tag{33}$$

Eqs. (31) and (32) are two decoupled steady-state advection-dispersion equations. The next step is to find explicit solutions of these two independent equations.

The solution of Eq. (31) is given as

$$\bar{b}_1(x,s) = A_1 e^{m_1 x} + B_1 e^{m_2 x} + \frac{b_{1,\text{init}}}{s}\,, \tag{34}$$

where,

$$m_{1,2} = \frac{Pe_m \pm \sqrt{Pe_m^2 + 4sPe_m\lambda_1}}{2}\,. \tag{35}$$

Similarly, the solution of Eq. (32) is expressed as

$$\bar{b}_2(x,s) = A_2 e^{n_1 x} + B_2 e^{n_2 x} + \frac{b_{2,\text{init}}}{s}\,, \tag{36}$$

where,

$$n_{1,2} = \frac{Pe_e \pm \sqrt{Pe_e^2 + 4sPe_e\lambda_2}}{2}\,. \tag{37}$$

Here A_1, A_2, B_1, and B_2 are constants of integration which can be obtained from the considered BCs at the column inlet and outlet.

The Laplace transformations of BCs in Eqs. (20a) and (20b) are given as

$$\bar{c_1}(0,s) = \frac{c_{1,\text{inj}}}{s}(1 - e^{-s\tau_{\text{inj}}})\,, \quad \frac{\partial \bar{c_1}(\infty,s)}{\partial x} = 0\,, \tag{38}$$

$$\bar{c_2}(0,s) = \frac{c_{2,\text{inj}}}{s}(1 - e^{-s\tau_{\text{inj}}})\,, \quad \frac{\partial \bar{c_2}(\infty,s)}{\partial x} = 0\,. \tag{39}$$

Transforming the above equations into $\bar{b}$-domain, we get

$$\bar{b}_1(0,s) = \frac{(1 - e^{-s\tau_{\text{inj}}})}{s\alpha(\lambda_1 - \lambda_2)}\left(\alpha c_{1,\text{inj}} - (\lambda_2 - \beta_e)c_{2,\text{inj}}\right)\,, \quad \frac{\partial \bar{b}_1}{\partial x}(\infty,s) = 0\,, \tag{40}$$

$$\bar{b}_2(0,s) = \frac{(1 - e^{-s\tau_{\text{inj}}})}{s\alpha(\lambda_2 - \lambda_1)}\left(\alpha c_{1,\text{inj}} - (\lambda_1 - \beta_e)c_{2,\text{inj}}\right)\,, \quad \frac{\partial \bar{b}_2}{\partial x}(\infty,s) = 0\,. \tag{41}$$

Using Eqs. (40) and (41), the values of A_1, A_2, B_1, and B_2 in Eqs. (34) and (36) take the following forms

$$A_1 = 0, \quad A_2 = 0, \quad B_1 = \bar{b}_1(0,s) - \frac{b_{1,\text{init}}}{s}, \quad B_2 = \bar{b}_2(0,s) - \frac{b_{2,\text{init}}}{s}. \tag{42}$$

On plugging the values of A_1 and B_1 in Eq. (34) and A_2 and B_2 in Eq. (36), we get

$$\bar{b}_1(x,s) = \left\{ \frac{(1-e^{-s\tau_{\text{inj}}})}{s\alpha(\lambda_1-\lambda_2)} \left(\alpha c_{1,\text{inj}} - (\lambda_2-\beta_e)c_{2,\text{inj}}\right) \right\} e^{m_2 x} + \frac{b_{1,\text{init}}}{s}\left(1-e^{m_2 x}\right) , \tag{43}$$

$$\bar{b}_2(x,s) = \left\{ \frac{(1-e^{-s\tau_{\text{inj}}})}{s\alpha(\lambda_2-\lambda_1)} \left(\alpha c_{1,\text{inj}} - (\lambda_1-\beta_e)c_{2,\text{inj}}\right) \right\} e^{n_2 x} + \frac{b_{2,\text{init}}}{s}\left(1-e^{n_2 x}\right) . \tag{44}$$

Now, using the transformations in Eq. (30), we get the Laplace domain solutions as

$$\begin{aligned}
\bar{c_1}(x,s) =& \frac{c_{1,\text{inj}}(1-e^{-s\tau_{\text{inj}}})}{s(\lambda_1-\lambda_2)}\left[(\lambda_1-\beta_e)e^{m_2 x} - (\lambda_2-\beta_e)e^{n_2 x}\right] + \frac{b_{1,\text{init}}(\lambda_1-\beta_e)}{s}(1-e^{m_2 x}) \\
&- \frac{\lambda_2-\beta_e}{s}\left[\frac{c_{2,\text{inj}}(\lambda_1-\beta_e)(1-e^{-s\tau_{\text{inj}}})}{\alpha(\lambda_1-\lambda_2)}\left(e^{m_2 x}-e^{n_2 x}\right) - b_{2,\text{init}}(1-e^{n_2 x})\right], \qquad (45) \\
\bar{c_2}(x,s) =& \frac{c_{1,\text{inj}}(1-e^{-s\tau_{\text{inj}}})\alpha}{s(\lambda_1-\lambda_2)}\left(e^{m_2 x}-e^{n_2 x}\right) + \frac{\alpha b_{1,\text{init}}}{s}(1-e^{m_2 x}) \\
&- \frac{c_{2,\text{inj}}(1-e^{-s\tau_{\text{inj}}})}{s(\lambda_1-\lambda_2)}\left[(\lambda_2-\beta_e)e^{m_2 x} - (\lambda_1-\beta_e)e^{n_2 x}\right] + \frac{\alpha b_{2,\text{init}}}{s}(1-e^{n_2 x}). \qquad (46)
\end{aligned}$$

The solution $c_j(x,\tau)$, $j = 1, 2$, in actual time domain is obtained by using the exact back transformation formula:

$$c_j(x,\tau) = \frac{1}{2\pi i}\int_{\zeta-i\infty}^{\zeta+i\infty} e^{-\tau s}\bar{c}_j(x,s)ds\,, \tag{47}$$

where, ζ is a real constant that exceeds the real part of all the singularities of $\bar{c_1}(x,s)$. On

applying Eq. (47) to Eqs. (45) and (46), we obtain

$$c_1(x,\tau) = \begin{cases} (\lambda_1-\beta_e)\left(\frac{c_{1,\mathrm{inj}}}{(\lambda_1-\lambda_2)} - \frac{c_{2,\mathrm{inj}}(\lambda_2-\beta_e)}{\alpha(\lambda_1-\lambda_2)} - b_{1,\mathrm{init}}\right)\eta_1(x,\tau) - (\lambda_2-\beta_e) \\ \left(\frac{c_{1,\mathrm{inj}}}{(\lambda_1-\lambda_2)} - \frac{c_{2,\mathrm{inj}}(\lambda_1-\beta_e)}{\alpha(\lambda_1-\lambda_2)} + b_{2,\mathrm{init}}\right)\eta_2(x,\tau) + (\lambda_1-\beta_e)b_{1,\mathrm{init}} \\ +(\lambda_2-\beta_e)b_{2,\mathrm{init}}, \qquad \text{if } 0 \le \tau \le \tau_{\mathrm{inj}}, \\ (\lambda_1-\beta_e)\left(\frac{c_{\mathrm{inj}}}{(\lambda_1-\lambda_2)} - \frac{c_{2,\mathrm{inj}}(\lambda_2-\beta_e)}{\alpha(\lambda_1-\lambda_2)} - b_{1,\mathrm{init}}\right)\eta_1(x,\tau) \\ -(\lambda_2-\beta_e)\left(\frac{c_{1,\mathrm{inj}}}{(\lambda_1-\lambda_2)} - \frac{c_{2,\mathrm{inj}}(\lambda_1-\beta_e)}{\alpha(\lambda_1-\lambda_2)} + b_{2,\mathrm{init}}\right)\eta_2(x,\tau) \\ -\frac{(\lambda_1-\beta_e)}{\alpha(\lambda_1-\lambda_2)}\left(\alpha c_{1,\mathrm{inj}} - (\lambda_2-\beta_e)c_{2,\mathrm{inj}}\right)\eta_1(x,\tau-\tau_{\mathrm{inj}}) \\ +\frac{(\lambda_2-\beta_e)}{\alpha(\lambda_1-\lambda_2)}\left(\alpha c_{1,\mathrm{inj}} - (\lambda_1-\beta_e)c_{2,\mathrm{inj}}\right)\eta_2(x,\tau-\tau_{\mathrm{inj}}) \\ +(\lambda_1-\beta_e)b_{1,\mathrm{init}} + (\lambda_2-\beta_e)b_{2,\mathrm{init}}, \qquad \text{if } \tau > \tau_{\mathrm{inj}}. \end{cases} \tag{48}$$

$$c_2(x,\tau) = \begin{cases} \left(\frac{c_{1,\mathrm{inj}}\alpha}{(\lambda_1-\lambda_2)} - \frac{c_{2,\mathrm{inj}}(\lambda_2-\beta_e)}{(\lambda_1-\lambda_2)} - \alpha b_{1,\mathrm{init}}\right)\eta_1(x,\tau) \\ -\left(\frac{c_{1,\mathrm{inj}}\alpha}{(\lambda_1-\lambda_2)} - \frac{c_{2,\mathrm{inj}}(\lambda_1-\beta_e)}{(\lambda_1-\lambda_2)} + \alpha b_{2,\mathrm{init}}\right)\eta_2(x,\tau) \\ +\alpha b_{1,\mathrm{init}} + \alpha b_{2,\mathrm{init}}, \qquad \text{if } 0 \le \tau \le \tau_{\mathrm{inj}}, \\ \left(\frac{c_{1,\mathrm{inj}}\alpha}{(\lambda_1-\lambda_2)} - \frac{c_{2,\mathrm{inj}}(\lambda_2-\beta_e)}{(\lambda_1-\lambda_2)} - \alpha b_{1,\mathrm{init}}\right)\eta_1(x,\tau) \\ -\left[\frac{c_{1,\mathrm{inj}}\alpha}{(\lambda_1-\lambda_2)} - \frac{c_{2,\mathrm{inj}}(\lambda_1-\beta_e)}{(\lambda_1-\lambda_2)} + \alpha b_{2,\mathrm{init}}\right]\eta_2(x,\tau) \\ -\frac{1}{(\lambda_1-\lambda_2)}\left(\alpha c_{1,\mathrm{inj}} - (\lambda_2-\beta_e)c_{2,\mathrm{inj}}\right)\eta_1(x,\tau-\tau_{\mathrm{inj}}) \\ +\frac{1}{(\lambda_1-\lambda_2)}\left(\alpha c_{1,\mathrm{inj}} - (\lambda_1-\beta_e)c_{2,\mathrm{inj}}\right)\eta_2(x,\tau-\tau_{\mathrm{inj}}) \\ +(\lambda_1-\beta_e)b_{1,\mathrm{init}} + (\lambda_2-\beta_e)b_{2,\mathrm{init}}. \qquad \text{if } \tau > \tau_{\mathrm{inj}}. \end{cases} \tag{49}$$

Here, η_1 and η_2 are given as

$$\eta_1(x,\tau) = \frac{1}{2}\mathrm{erfc}\left[\frac{\sqrt{Pe_m}(\lambda_1 x-\tau)}{2\sqrt{\lambda_1\tau}}\right] + \frac{1}{2}e^{Pe_m x}\mathrm{erfc}\left[\frac{\sqrt{Pe_m}(\lambda_1 x+\tau)}{2\sqrt{\lambda_1\tau}}\right], \tag{50}$$

$$\eta_2(x,\tau) = \frac{1}{2}\mathrm{erfc}\left[\frac{\sqrt{Pe_e}(\lambda_2 x-\tau)}{2\sqrt{\lambda_2\tau}}\right] + \frac{1}{2}e^{Pe_e x}\mathrm{erfc}\left[\frac{\sqrt{Pe_e}(\lambda_2 x+\tau)}{2\sqrt{\lambda_2\tau}}\right]. \tag{51}$$

4. Moments analysis

Analytical expression of the first four temporal moments are derived from the Laplace-transformed solutions of the mass and energy balances based on the linearized equilibrium condition (Eq. (12)). These moments are very useful to analyze peaks areas (masses), retention times, band broadenings, front asymmetries, and kurtosises of the concentration and temperature profiles. It is well known that requirements on the precision of measured elution profiles increase quickly for calculations of higher order moments. Third moments are typically still accessible with the current detection tools. Fourth moments are typically very difficult to quantify.

In order to calculate analytical moments for rectangular concentration pulses of finite width, the following moment generating property of the Laplace transform is exploited for $\bar{w} \in \{\bar{c_1}, \bar{c_2}\}$:

$$M_{0,w} = \frac{L}{u} \lim_{s \to 0} (\bar{w}(x = 1, s)), \quad M_{n,w} = \left(-\frac{L}{u}\right)^n \lim_{s \to 0} \frac{d^n(\bar{w}(x = 1, s))}{ds^n}, \quad n = 1, 2, \cdots . \tag{52}$$

Moreover, it is assumed that column is initially regenerated and has a reference temperature, i.e.

$$c_{1,\text{init}} = 0, \quad c_{2,\text{init}} = 0 \,. \tag{53}$$

The first four moments are derived using the Laplace-transformed solutions in Eqs. (45) and (46). The zeroth, first and second moments of c_1 and c_2 are presented below, while the remaining third and fourth moments are given in Appendix A.

Zeroth moments: The zeroth moments of c_1 and c_2 are expressed as

$$\mathbf{M}_0 = \begin{pmatrix} M_{0,c_1} \\ \\ M_{0,c_2} \end{pmatrix} = \begin{pmatrix} c_{1,\mathrm{inj}} t_{\mathrm{inj}} \\ \\ c_{2,\mathrm{inj}} t_{\mathrm{inj}} \end{pmatrix}. \tag{54}$$

First moments: The first temporal moments are given as

$$\mathbf{M}_1 = \begin{pmatrix} M_{1,c_1} \\ \\ M_{1,c_2} \end{pmatrix} = \begin{pmatrix} \mu_{11}^1 & \mu_{12}^1 \\ \\ \mu_{21}^1 & \mu_{22}^1 \end{pmatrix} \begin{pmatrix} M_{0,c_1} \\ \\ M_{0,c_2} \end{pmatrix}, \tag{55}$$

were

$$\mu_{11}^1 = \frac{t_{\mathrm{inj}}}{2} + \frac{L}{u}\beta_m, \quad \mu_{12}^1 = \frac{L}{u}\gamma\,, \quad \mu_{21}^1 = \frac{L}{u}\alpha, \quad \mu_{22}^1 = \frac{t_{\mathrm{inj}}}{2} + \frac{L}{u}\beta_e. \tag{56}$$

Here, β_m, β_e α, and γ are given by Eqs. (16) and (17). Moreover, $\mu_{1,ij}$ denotes the mean retention time of component i due input variation of component j.

It can be observed in Eq. (56) that β_m and β_e describe the mean retention times of concentration pulse and temperature wave inside the column (which are reciprocals of the two characteristics speeds), respectively. For a Dirac pulse injection, we obtain (c.f. Eqs. (16) and (17))

$$\frac{\mu_{11}^1}{\mu_{22}^1} = \frac{\beta_m}{\beta_e} = \frac{1 + F a_{\mathrm{ref}}}{1 + F\frac{\rho^S c_p^S}{\rho^L c_p^L} + F\frac{\Delta H_A^2 a_{\mathrm{ref}} c_{\mathrm{ref}}}{R_g T_{\mathrm{ref}}^2 \rho^L c_p^L}}\,. \tag{57}$$

If $\beta_m/\beta_e = 1$ then the both concentration pulse and temperature wave are coupled, otherwise they are decoupled.

Second moments: The second moments are given as

$$\mathbf{M}_2 = \begin{pmatrix} M_{2,c_1} \\ \\ M_{2,c_2} \end{pmatrix} = \begin{pmatrix} \mu_{11}^2 & \mu_{12}^2 \\ \\ \mu_{21}^2 & \mu_{22}^2 \end{pmatrix} \begin{pmatrix} M_{0,c_1} \\ \\ M_{0,c_2} \end{pmatrix}, \tag{58}$$

where

$$\mu_{11}^2 = \frac{t_{\text{inj}}^2}{3} + t_{\text{inj}}\frac{L}{u}\beta_m + \frac{L^2}{u^2}\left[(\beta_m^2+\alpha\gamma)\left(1+\frac{1}{Pe_m}+\frac{1}{Pe_e}\right) + \frac{\beta_m^3+\alpha\gamma\beta_e-\beta_m^2\beta_e+3\alpha\gamma\beta_m}{2\lambda_1-(\beta_m+\beta_e)}\left(\frac{1}{Pe_m}-\frac{1}{Pe_e}\right)\right], \quad (59)$$

$$\mu_{12}^2 = t_{\text{inj}}\frac{L}{u}\gamma + \frac{L^2}{u^2}\left[\gamma(\beta_m+\beta_e)\left(1+\frac{1}{Pe_m}+\frac{1}{Pe_e}\right) + \gamma\frac{\beta_m^2+\beta_e^2+2\alpha\gamma}{2\lambda_1-(\beta_m+\beta_e)}\left(\frac{1}{Pe_m}-\frac{1}{Pe_e}\right)\right], \quad (60)$$

$$\mu_{21}^2 = t_{\text{inj}}\frac{L}{u}\alpha + \frac{L^2}{u^2}\left[\alpha(\beta_m+\beta_e)\left(1+\frac{1}{Pe_m}+\frac{1}{Pe_e}\right) + \alpha\frac{\beta_m^2+\beta_e^2+2\alpha\gamma}{2\lambda_1-(\beta_m+\beta_e)}\left(\frac{1}{Pe_m}-\frac{1}{Pe_e}\right)\right], \quad (61)$$

$$\mu_{22}^2 = \frac{t_{\text{inj}}^2}{3} + t_{\text{inj}}\frac{L}{u}\beta_e + \frac{L^2}{u^2}\left[(\beta_e^2+\alpha\gamma)\left(1+\frac{1}{Pe_m}+\frac{1}{Pe_e}\right) + \frac{\beta_e^3+\alpha\gamma\beta_m-\beta_e^2\beta_m+3\alpha\gamma\beta_e}{2\lambda_1-(\beta_m+\beta_e)}\left(\frac{1}{Pe_m}-\frac{1}{Pe_e}\right)\right]. \quad (62)$$

Here, λ_1 is given by Eq. (25).

Second central moments: The second central moments are calculated as

$$\mathbf{M}_2' = [\sigma]\mathbf{M}_0 = \left([\mu^2]-[\mu^1]^2\right)\mathbf{M}_0, \quad (63)$$

where, [ ] denotes the 2×2 matrix. Thus, we obtain

$$\mathbf{M}_2' = \begin{pmatrix} M_{2,m}' \\ \\ M_{2,e}' \end{pmatrix} = \begin{pmatrix} \sigma_{11} & \sigma_{12} \\ \\ \sigma_{21} & \sigma_{22} \end{pmatrix}\begin{pmatrix} M_{0,m} \\ \\ M_{0,e} \end{pmatrix}, \quad (64)$$

where

$$\sigma_{11} = \frac{t_{\text{inj}}^2}{12} + \frac{L^2}{u^2}\left[(\beta_m^2+\alpha\gamma)\left(\frac{1}{Pe_m}+\frac{1}{Pe_e}\right) + \frac{\beta_m^3+\alpha\gamma\beta_e-\beta_m^2\beta_e+3\alpha\gamma\beta_m}{2\lambda_1-(\beta_m+\beta_e)}\left(\frac{1}{Pe_m}-\frac{1}{Pe_e}\right)\right], \quad (65)$$

$$\sigma_{12} = \frac{L^2}{u^2}\left[\gamma(\beta_m+\beta_e)\left(\frac{1}{Pe_m}+\frac{1}{Pe_e}\right) + \gamma\frac{\beta_m^2+\beta_e^2+2\alpha\gamma}{2\lambda_1-(\beta_m+\beta_e)}\left(\frac{1}{Pe_m}-\frac{1}{Pe_e}\right)\right], \quad (66)$$

$$\sigma_{21} = \frac{L^2}{u^2}\left[\alpha(\beta_m+\beta_e)\left(\frac{1}{Pe_m}+\frac{1}{Pe_e}\right) + \alpha\frac{\beta_m^2+\beta_e^2+2\alpha\gamma}{2\lambda_1-(\beta_m+\beta_e)}\left(\frac{1}{Pe_m}-\frac{1}{Pe_e}\right)\right], \quad (67)$$

$$\sigma_{22} = \frac{t_{\text{inj}}^2}{12} + \frac{L^2}{u^2}\left[(\beta_e^2+\alpha\gamma)\left(\frac{1}{Pe_m}+\frac{1}{Pe_e}\right) + \frac{\beta_e^3+\alpha\gamma\beta_m-\beta_e^2\beta_m+3\alpha\gamma\beta_e}{2\lambda_1-(\beta_m+\beta_e)}\left(\frac{1}{Pe_m}-\frac{1}{Pe_e}\right)\right]. \quad (68)$$

Here, σ_{ij} indicates the mean variance of component i due to input variation of component j.

The analytical expression of third and fourth moments are presented in Appendix A.

In the case of very wide pulse injections (i.e. $t_{\text{inj}} \to \infty$), one has to use the derivatives of $\bar{w}$ with respect to s in Eq. (52). Then, the t_{inj} terms on the right hand sides of μ_{ii}^{j}, for $i, j = 1, 2, 3, 4$, will disappear.

5. Numerical case studies

Several case studies are considered to generate and analyze concentration and temperature profiles predicted using the derived solutions. To compare and evaluate the validity of the linearization of the equilibrium function, a second order accurate finite volume scheme (FVS) is applied to numerically approximate the nonlinear model (c.f. Eqs. (9), (10) and (3) instead of using the linearized Eq. (12)). The reference parameters used in test problems are summarized in Table 1.

5.1. Effect of enthalpy of adsorption ΔH_A for $T_{\text{inj}} = T_{\text{init}}$ ("matching" injection)

Figures 1 displays the results for an isothermal case (selecting $\Delta H_A = 0$) compared to a non-isothermal case (considering ΔH_A). Hereby both inlet and initial temperatures had the reference values ($T_{\text{inj}} = T_{\text{init}} = T_{\text{ref}}$). It is confirmed in Figure 1(a) that no change in the temperature occurs if the enthalpy of adsorption is not considered. In contrast, as shown in Figure 1(b), the enthalpy of adsorption has already a significant effect on the temperature profile c_2 for a moderate enthalpy of $-10\,kJ/mol$ without causing a pronounced change in the concentration profile c_1. Moreover, it can be noticed that the first eluting adsorption front produces first a well recognizable rise in the temperature profile ($> 1.5\,K$). Afterwards desorption takes place connected with a reduction of the

temperature. Finally, the temperature attains again its reference value. Because of the chosen values of reference parameters building up β_m and β_e, we obtain $\beta_m = \beta_e$. In this particular case, the concentration and temperature fronts are moving with very similar speed and the mean retention times of concentration and temperature profiles are the same (c.f. Eq. (56)), i.e. $\mu_{11}^1 = \mu_{22}^1 = 13\,min$. Moreover, due to the coupling of concentration pulse and temperature wave, the values of the corresponding second, third and fourth central moments (c.f. Eqs. (65), (68), (A-8), (A-11), (A-19), (A-22)) are also the same, i.e $\sigma_{11} = \sigma_{22} = 3.21\,min^2$, $\delta_{11} = \delta_{22} = 2.34\,min^3$, and $\kappa_{11} = \kappa_{22} = 33.80\,min^4$.

Figures 2 and 3 show the concentration and temperature profiles at different values of ΔH_A. It can be observed that the analytical solutions for the linearized isotherm model (c.f. Eq. (12)) and the numerical solutions of HR-FVS for the nonlinear isotherm equilibrium function (c.f. Eq. (3)) start deviating from each other when the enthalpies of adsorption, $|\Delta H_A|$, increase above $10\,kJ/mol$. Such larger enthalpies of adsorption are the source for more significant temperature fluctuations. The results clearly endorse our assumptions regarding the linearization of isotherm for moderate adsorption enthalpies. For an enthalpy of $-40\,kJ/mol$ there are already predicted temperature deviations exceeding $4K$ (Figure 3). Our analytical solution overestimates the deviation from isothermal behavior compared to the more precise numerical solution.

5.2. Effect of "non-matching" injection temperature ($T_{\mathrm{inj}} \neq T_{\mathrm{init}}$)

Figure 4 demonstrates the effects of varying the temperature of the injected sample on the courses of the concentration and temperature profiles. In Figure 4(a), it can be seen that the

first eluting adsorption peak of the temperature rises due to a "hot injection" ($T_{\text{inj}} > T_{\text{init}}$). The later occurring temperature drop due to endothermic desorption gradually shrinks in the case of increased injection temperatures ($310K$ vs. $300K$). On the other hand, as shown in Figure 4(b), the desorption peak of the temperature profile goes further down in the case of a "cold injection" ($T_{\text{inj}} < T_{\text{init}}$). In such cases exothermal adsorption peak diminish.

Considering both cases of injection temperature deviations it should be noted, that due to the relative low adsorption enthalpy considered and the corresponding small temperature amplitudes, there is no visible effect of the injection temperature deviations on the concentration profiles. Once again, because of $\beta_m = \beta_e$ used here, both concentration and temperature profiles are moving at the same speed, i.e. they are coupled. Thus, the corresponding moments of concentration and temperature have the same values as observed in the case introduced above in Subsection 5.1.

5.3. Effect of the ratio β_m/β_e

Figure 5 shows the effects of varying the ratio β_m/β_e (considered in the calculations reported above to be unity) on the concentration and temperature profiles for $T_{\text{inj}} = T_{\text{init}}$. This ratio describes the retention time of concentration pulse versus temperature wave (c.f. Eq. (57)) and is for that reason elaborated in more detail.

In Figure 5(a)), we have taken the ratio β_m/β_e as 0.156 obtained by considering $\rho^S c_p^S = 40\,kJ/lK$ and keeping $\rho^L c_p^L = 4\,kJ/lK$. For such ratios, the speed of the concentration profiles is larger than the speed of the thermal profiles. Thus, the adsorption related

positive peaks of temperature are coupled with the faster moving concentration profiles. In contrast, the slower and decoupled negative desorption peaks of the temperature leave the column later. For the case study considered, the values of mean retention times are $\mu_{11}^1 = 13\,min$ and $\mu_{22}^1 = 80.5\,min$. Herby, μ_{11}^1 describes the mean retention time of the coupled first concentration and temperature adsorption peaks. On the other hand, μ_{22}^1 denotes the mean retention time of the decoupled desorption related temperature peak (Figure 5(a)). Moreover, $\sigma_{11} = 3.21\,min^2$ represents the variance of the coupled concentration and temperature (adsorption) peaks, while, $\sigma_{22} = 128.1\,min^2$ denotes the variance of the decoupled temperature desorption peak.

Figure 5(b) gives corresponding plots of the profiles for $\beta_m/\beta_e = 2.174$ obtained by using $\rho^S c_p^S = 4\,kJ/lK$ and $\rho^L c_p^L = 40\,kJ/lK$ as hypothetical values. In this not realistic case, the speed of the temperature profile is faster than that of the concentration profile. Thus, the positive adsorption peak of the temperature profile is decoupled and moves ahead. Now, the negative temperature peak caused by desorption is coupled with the concentration profile, i.e. these two perturbations move at the same speed. In this case, $\mu_{11}^1 = 13\,min$ denotes the retention time of coupled concentration and temperature desorption peaks. On the other hand, $\mu_{22}^1 = 6.25\,min$ denotes the smaller retention time of the decoupled temperature adsorption peak (see Figure 5(b)). Moreover, the variance of the coupled slow peaks of concentration and temperature is $\sigma_{11} = 3.21\,min^2$, while the variance of the faster temperature adsorption peak is just $\sigma_{22} = 0.15\,min^2$.

Figures 6(a)&(b) show the plots of concentration profiles and temperature waves for different values of the reference Henry's constant a_{ref}, while keeping again $\rho^S c_p^S = 40$ and

$\rho^L c_p^L = 4$ fixed. It can be observed that now the concentration profiles are shifted towards larger retention times for larger a_{ref} connected with increased band broadening. On the other hand, the amplitudes of temperature fluctuations increase until $a_{\text{ref}} = 10$ and then decrease. At $a_{\text{ref}} = 10$ both concentration and temperature profiles are moving at the same speed, both are coupled because of $\beta_m/\beta_e = 1$. For $a_{\text{ref}} \lesseqgtr 10$, the concentration and temperature fronts are decoupled. Figure 6(c) gives the plot of the maximum positive temperature change versus a_{ref}. It can be seen that the temperature fluctuations reach to an extremum of $0.41\,K$ during the prefect coupling of the two fronts for $a_{\text{ref}} = 10$.

5.4. Effect of "hot injections" for $\beta_m/\beta_e \lesseqgtr 1$

In contrast to the above results, Figure 7 illustrates the joint effects of non-matching ("hot") injection temperatures ($T_{\text{inj}} > T_{\text{init}}$) and ratios β_m/β_e differing from unity. It can be seen that the type of adsorption and desorption coupling obtained for matching injection temperatures (Figure 5(a)) remains the same. However, as shown in Figure 7(a) for $\beta_m/\beta_e = 0.156$, the increased injection temperature lifts up the temperature profile related to the desorption peak leaving the corresponding adsorption peak unaffected. In contrast, for $\beta_m/\beta_e = 2.174$, the higher injection temperature enhances the temperature profile related to the adsorption peak and has no effect on the corresponding desorption peak (Figure 7(b)).

5.5. Effects of axial dispersion (parameters Pe_m and Pe_e)

The specific effects of the two Peclet numbers Pe_m (describing axial dispersion) and Pe_e (describing axial heat conductivity) (c.f. Eq. (8)) on the concentration and temperature

profiles are illustrated in Figure 8 for two different values of ratio β_m/β_e keeping $T_{\text{inj}} = T_{\text{init}}$. In Figures 8(a) and 8(c) the effect of Pe_m is studied for a fixed value of $Pe_e = 100$. The variation of Pe_m has a pronounced effect only if the concentration and temperature peaks are coupled, while it has no effect on the separated decoupled temperature peak. The coupled peaks of concentration and temperature clearly become broader on decreasing the value of Pe_m (i.e. on increasing D_z).

On the other hand, Figures 8(b) and 8(d) show the influence of Pe_e (which includes the axial heat conductivity coefficient λ_z, c.f. Eq. (8)) on the concentration and temperature profiles for fixed $Pe_m = 100$. It can be seen that Pe_e only effects the decoupled temperature peaks, while it has no effect on the coupled concentration and temperature peaks. The decoupled temperature peaks become broadened on decreasing the value of Pe_e (i.e. for increased λ_z).

Figures 9 and 10 show the effects of Pe_m and Pe_e on the first four moments (Eqs. (56), (65), (68), (A-8), (A-11), (A-19), (A-22)) representing retention time, variance, skewness and kurtosis of the profiles. In the calculations reported we have chosen the ratio $\beta_m/\beta_e < 1\,(= 0.156)$ using realistic orders of magnitude for $\rho^S c_p^S\,(= 40)$ and $\rho^L c_p^L\,(= 4)$. It can be observed that, as required, both Peclect numbers have no effect on the mean retention times (μ_{11}^1 and μ_{22}^1). On the other hand, the variances (σ_{11} and σ_{22}), skewnesses (δ_{11} and δ_{22}), and kurtosises (κ_{11} and κ_{22}) are either constant or decrease on increasing the values of Pe_m or Pe_e. These plotted curves correctly reflect the behaviors of the elution curves displayed in Figures 8(a) and 8(b).

Of particular interest for chromatographic separation processes are the second moments

frequently considered as a measure of "column efficiencies" or "heights equivalent to theoretical plates (HETP)" (e.g. Guiochon et al. (2006)) which are discussed in the next section.

5.6. Effect of u on HETP curves

Figure 11(a) shows plots of HETP-values as a function of the linear velocity for three different values of the ratio β_m/β_e. Two types of HETP-values corresponding to the specific EDM used in this paper were calculated according to the following classical equations Van Deemter et al. (1956); Guiochon et al. (2006)):

$$\mathrm{HETP}_m = \frac{L\sigma_{11}}{(\mu_{11}^1)^2}, \tag{69}$$

$$\mathrm{HETP}_e = \frac{L\sigma_{22}}{(\mu_{22}^1)^2}. \tag{70}$$

In the calculations performed and illustrated in Figure 11 we took as reasonable values $D_z = 0.002\, cm^2 min^{-1}$ and $\lambda_z = 0.008\, kJ cm^{-1} min^{-1}$. All plots shown in Figure 11(a) reveal the typical classical shape of such efficiency curves, indicating that there is a certain flow rate at which HETP reaches a minimum and the efficiency a maximum. The shown three courses of the mass balance (concentration) related HETP_m-curves are identical for the different ratios of β_m/β_e. In the case that this ratio is unity, due to the coherently traveling concentration and temperature profile, also the HETP_e-curve (which evaluates the width of the temperature profile) corresponds to the HETP_m-curves. However, the HETP_e-curves differ for pronounced decoupling of one of the temperature peaks, as shown for $\beta_m/\beta_e = 0.156$ and $\beta_m/\beta_e = 2.174$. This means that the variance of this second decoupled

peaks carries valuable specific information about Pe_e and, thus, the axial heat conductivity coefficient λ_z. The lower part of Figure 11 shows for demonstration predicted elution profiles for $u = 1\,cm/min$ using the two mentioned ratios 0.156 and 2.174. In agreement with the HETP-curves, in case of a ratio $\beta_m/\beta_e = 2.174$ the first eluting (separated) temperature peak is clearly broadened to an "unusual" degree due to the larger HETP_e-value, which exceeds HETP_m, see Figure 11(c).

6. Conclusion

The model equations of a linearized non-isothermal equilibrium dispersive model (EDM) of adiabatic liquid chromatography were solved analytically in order to quantify thermal effects in chromatographic columns. The solution process successively employed Laplace transformation and linear transformation steps to uncouple the governing set of coupled differential equations. The resulting uncoupled system of ordinary differential equations was solved using an elementary solution technique. The derived new analytical solutions are considered to be very useful to understand and analyze dynamic concentration and thermal fronts in chromatographic columns in case of relative small deviations from isothermal behavior. For deeper analysis of the process, the moment generating property of the Laplace domain solutions was utilized to derive instructive analytical expressions of the first four temporal moments of the concentration and temperature profiles. These moment expressions are seen as very valuable for the understanding of front traveling phenomena and for the identification of model parameters from experimentally determined column outlet concentration and temperature profiles. Application would require a careful recording

of the small temperature fluctuations which is typically not practiced. There are option available as described by Brandt et al. (1997); Sainio (2005, 2007). Expressions for the higher moments of the temperature responses have not been available before. Applying reasonable model parameters several case studies were considered. To critically validate the solutions and the linear assumptions mode, the analytical solutions for linearized isotherm were successfully compared with numerical results using a high resolution finite volume scheme considering more realistic nonlinear isotherms. The solutions derived in this paper can be used in more systematic studies to determine general criteria which would allow predicting maximum deviations from the isothermal behavior and offering a rational basis for eventually reducing the model again to an isothermal one.

Appendix A

Here, the analytical expressions of third and fourth moments are presented.

Third moments: The third moments are given as

$$\mathbf{M}_3 = \begin{pmatrix} M_{3,m} \\ \\ M_{3,e} \end{pmatrix} = \begin{pmatrix} \mu_{11}^3 & \mu_{12}^3 \\ \\ \mu_{21}^3 & \mu_{22}^3 \end{pmatrix} \begin{pmatrix} M_{0,m} \\ \\ M_{0,e} \end{pmatrix}, \tag{A-1}$$

where for given λ_1 in Eq. (25)

$$\begin{aligned}
\mu_{11}^3 =& \frac{t_{\text{inj}}^3}{4} + t_{\text{inj}}^2 \frac{L}{u}\beta_m + \frac{3t_{\text{inj}}}{2}\frac{L^2}{u^2}\left[(\beta_m^2 + \alpha\gamma)\left(1 + \frac{1}{Pe_m} + \frac{1}{Pe_e}\right) + \frac{\beta_m^3 + 3\alpha\gamma(\beta_m + \beta_e) - \beta_m^2\beta_e}{2\lambda_1 - (\beta_m + \beta_e)}\right. \\
& \left.\left(\frac{1}{Pe_m} - \frac{1}{Pe_e}\right)\right] + \frac{L^3}{u^3}\left[(\beta_m^3 + \alpha\gamma\beta_e + 2\beta_m\alpha\gamma)\left(1 + \frac{3}{Pe_m} + \frac{3}{Pe_e} + \frac{6}{Pe_m^2} + \frac{6}{Pe_e^2}\right)\right. \\
& \left. + \frac{\beta_m^4 - \beta_m^3\beta_e + \alpha\gamma\beta_e^2 + 4\beta_m^2\alpha\gamma + 2\alpha^2\gamma^2 + \beta_m\alpha\gamma\beta_e}{2\lambda_1 - (\beta_m + \beta_e)}\left(\frac{3}{Pe_m} - \frac{3}{Pe_e} + \frac{6}{Pe_m^2} - \frac{6}{Pe_e^2}\right)\right], \qquad \text{(A-2)} \\
\mu_{12}^3 =& t_{\text{inj}}^2 \frac{L}{u}\gamma + \frac{3}{2}t_{\text{inj}}\frac{L^2}{u^2}\left[\gamma(\beta_m + \beta_e)\left(1 + \frac{1}{Pe_m} + \frac{1}{Pe_e}\right) + \gamma\frac{\beta_m^2 + \beta_e^2 + 2\alpha\gamma}{2\lambda_1 - (\beta_m + \beta_e)}\left(\frac{1}{Pe_m} - \frac{1}{Pe_e}\right)\right] \\
& + \frac{L^3}{u^3}\left[\gamma(\beta_m^2 + \beta_e^2 + \alpha\gamma + \beta_m\beta_e)\left(1 + \frac{3}{Pe_m} + \frac{3}{Pe_e} + \frac{6}{Pe_m^2} + \frac{6}{Pe_e^2}\right)\right.
\end{aligned}$$

$$+\gamma\frac{\beta_m^3+\beta_e^3+3\alpha\gamma(\beta_m+\beta_e)}{2\lambda_1-(\beta_m+\beta_e)}\left(\frac{3}{Pe_m}-\frac{3}{Pe_e}+\frac{6}{Pe_m^2}-\frac{6}{Pe_e^2}\right)\Bigg], \tag{A-3}$$

$$\begin{aligned}\mu_{21}^3 =&t_{\text{inj}}^2\frac{L}{u}\alpha+\frac{3}{2}t_{\text{inj}}\frac{L^2}{u^2}\left[\alpha(\beta_m+\beta_e)\left(1+\frac{1}{Pe_m}+\frac{1}{Pe_e}\right)+\alpha\frac{\beta_m^2+\beta_e^2+2\alpha\gamma}{2\lambda_1-(\beta_m+\beta_e)}\left(\frac{1}{Pe_m}-\frac{1}{Pe_e}\right)\right]\\&+\frac{L^3}{u^3}\Bigg[\alpha(\beta_m^2+\beta_e^2+\alpha\gamma+\beta_m\beta_e)\left(1+\frac{3}{Pe_m}+\frac{3}{Pe_e}+\frac{6}{Pe_m^2}+\frac{6}{Pe_e^2}\right)\\&+\alpha\frac{\beta_m^3+\beta_e^3+3\alpha\gamma(\beta_m+\beta_e)}{2\lambda_1-(\beta_m+\beta_e)}\left(\frac{3}{Pe_m}-\frac{3}{Pe_e}+\frac{6}{Pe_m^2}-\frac{6}{Pe_e^2}\right)\Bigg],\end{aligned} \tag{A-4}$$

$$\begin{aligned}\mu_{22}^3 =&\frac{t_{\text{inj}}^3}{4}+t_{\text{inj}}^2\frac{L}{u}\beta_e+\frac{3t_{\text{inj}}}{2}\frac{L^2}{u^2}\Bigg[(\beta_e^2+\alpha\gamma)\left(1+\frac{1}{Pe_m}+\frac{1}{Pe_e}\right)+\frac{\beta_e^3+3\alpha\gamma(\beta_e+\beta_m)-\beta_e^2\beta_m}{2\lambda_1-(\beta_m+\beta_e)}\\&\left(\frac{1}{Pe_m}-\frac{1}{Pe_e}\right)\Bigg]+\frac{L^3}{u^3}\Bigg[(\beta_e^3+\alpha\gamma\beta_m+2\beta_e\alpha\gamma)\left(1+\frac{3}{Pe_m}+\frac{3}{Pe_e}+\frac{6}{Pe_m^2}+\frac{6}{Pe_e^2}\right)\\&+\frac{\beta_e^4-\beta_e^3\beta_m+\alpha\gamma\beta_m^2+4\beta_e^2\alpha\gamma+2\alpha^2\gamma^2+\beta_e\alpha\gamma\beta_m}{2\lambda_1-(\beta_m+\beta_e)}\left(\frac{3}{Pe_m}-\frac{3}{Pe_e}+\frac{6}{Pe_m^2}-\frac{6}{Pe_e^2}\right)\Bigg].\end{aligned} \tag{A-5}$$

Third central moments: The third central moment is calculated as

$$\mathbf{M}_3'=[\delta]\mathbf{M}_0=\left([\mu^3]-3[\mu^1][\mu^2]+2[\mu^1]^3\right)\mathbf{M}_0. \tag{A-6}$$

Thus, we obtain

$$\mathbf{M}_3'=\begin{pmatrix}M_{3,m}'\\M_{3,e}'\end{pmatrix}=\begin{pmatrix}\delta_{11}&\delta_{12}\\\delta_{21}&\delta_{22}\end{pmatrix}\begin{pmatrix}M_{0,m}\\M_{0,e}\end{pmatrix}, \tag{A-7}$$

where

$$\begin{aligned}\delta_{11} =&\frac{L^3}{u^3}\Bigg[(\beta_m^3+\alpha\gamma\beta_e+2\beta_m\alpha\gamma)\left(\frac{6}{Pe_m^2}+\frac{6}{Pe_e^2}\right)\\&+\frac{\beta_m^4-\beta_m^3\beta_e+\alpha\gamma\beta_e^2+4\beta_m^2\alpha\gamma+2\alpha^2\gamma^2+\beta_m\alpha\gamma\beta_e}{2\lambda_1-(\beta_m+\beta_e)}\left(\frac{6}{Pe_m^2}-\frac{6}{Pe_e^2}\right)\Bigg],\end{aligned} \tag{A-8}$$

$$\delta_{12} =\frac{L^3}{u^3}\left[\gamma(\beta_m^2+\beta_e^2+\alpha\gamma+\beta_m\beta_e)\left(\frac{6}{Pe_m^2}+\frac{6}{Pe_e^2}\right)+\gamma\frac{\beta_m^3+\beta_e^3+3\alpha\gamma(\beta_m+\beta_e)}{2\lambda_1-(\beta_m+\beta_e)}\left(\frac{6}{Pe_m^2}-\frac{6}{Pe_e^2}\right)\right], \tag{A-9}$$

$$\delta_{21} =\frac{L^3}{u^3}\left[\alpha(\beta_m^2+\beta_e^2+\alpha\gamma+\beta_m\beta_e)\left(\frac{6}{Pe_m^2}+\frac{6}{Pe_e^2}\right)+\alpha\frac{\beta_m^3+\beta_e^3+3\alpha\gamma(\beta_m+\beta_e)}{2\lambda_1-(\beta_m+\beta_e)}\left(\frac{6}{Pe_m^2}-\frac{6}{Pe_e^2}\right)\right], \tag{A-10}$$

$$\begin{aligned}\delta_{22} =&\frac{L^3}{u^3}\Bigg[(\beta_e^3+\alpha\gamma\beta_m+2\beta_e\alpha\gamma)\left(\frac{6}{Pe_m^2}+\frac{6}{Pe_e^2}\right)\\&+\frac{\beta_e^4-\beta_e^3\beta_m+\alpha\gamma\beta_m^2+4\beta_e^2\alpha\gamma+2\alpha^2\gamma^2+\beta_e\alpha\gamma\beta_m}{2\lambda_1-(\beta_m+\beta_e)}\left(\frac{6}{Pe_m^2}-\frac{6}{Pe_e^2}\right)\Bigg].\end{aligned} \tag{A-11}$$

Fourth moments: The fourth moments are given as

$$\mathbf{M}_4 = \begin{pmatrix} M_{4,m} \\ \\ M_{4,e} \end{pmatrix} = \begin{pmatrix} \mu_{11}^4 & \mu_{12}^4 \\ \\ \mu_{21}^4 & \mu_{22}^4 \end{pmatrix} \begin{pmatrix} M_{0,m} \\ \\ M_{0,e} \end{pmatrix}, \tag{A-12}$$

where

$$\begin{aligned}
\mu_{11}^4 =& \frac{t_{\text{inj}}^4}{5} + t_{\text{inj}}^3 \frac{L}{u}\beta_m + 2t_{\text{inj}}^2 \frac{L^2}{u^2}\left[(\beta_m^2 + \alpha\gamma)\left(1 + \frac{1}{Pe_m} + \frac{1}{Pe_e}\right) + \frac{\beta_m^3 + 3\beta_m\alpha\gamma + \alpha\gamma\beta_e - \beta_m^2\beta_e}{2\lambda_1 - (\beta_m + \beta_e)}\right. \\
& \left.\left(\frac{1}{Pe_m} - \frac{1}{Pe_e}\right)\right] + 2\tau_{\text{inj}}\frac{L^3}{u^3}\left[(\beta_m^3 + \alpha\gamma\beta_e + 2\beta_m\alpha\gamma)\left(1 + \frac{3}{Pe_m} + \frac{3}{Pe_e} + \frac{6}{Pe_m^2} + \frac{6}{Pe_e^2}\right)\right. \\
& \left. + \frac{\beta_m^4 - \beta_m^3\beta_e + \alpha\gamma\beta_e^2 + 4\beta_m^2\alpha\gamma + 2\alpha^2\gamma^2 + \beta_m\alpha\gamma\beta_e}{2\lambda_1 - (\beta_m + \beta_e)}\left(\frac{3}{Pe_m} - \frac{3}{Pe_e} + \frac{6}{Pe_m^2} - \frac{6}{Pe_e^2}\right)\right] \\
& + \frac{L^4}{u^4}\left[(\alpha^2\gamma^2 + \beta_m^4 + \beta_e^2\alpha\gamma + 2\beta_m\alpha\beta_e\gamma + 3\beta_m^2\alpha\gamma)\left(1 + \frac{6}{Pe_m} + \frac{6}{Pe_e} + \frac{30}{Pe_m^2} + \frac{30}{Pe_e^2} + \frac{60}{Pe_m^3} + \frac{60}{Pe_e^3}\right)\right] \\
& + \frac{\beta_m^5 + \beta_e^3\alpha\gamma - \beta_m^4\beta_e + 5\beta_m^3\alpha\gamma + \beta_m\beta_e^2\alpha\gamma + 5\beta_m\alpha^2\gamma^2 + \beta_m^2\beta_e\alpha\gamma + 3\alpha^2\gamma^2\beta_e}{2\lambda_1 - (\beta_m + \beta_e)} \\
& \left.\left(\frac{6}{Pe_m} - \frac{6}{Pe_e} + \frac{30}{Pe_m^2} - \frac{30}{Pe_e^2} + \frac{60}{Pe_m^3} - \frac{60}{Pe_e^3}\right)\right],
\end{aligned} \tag{A-13}$$

$$\begin{aligned}
\mu_{12}^4 =& t_{\text{inj}}^3 \frac{L}{u}\gamma + 2t_{\text{inj}}^2 \frac{L^2}{u^2}\left[\gamma(\beta_m + \beta_e)\left(1 + \frac{1}{Pe_m} + \frac{1}{Pe_e}\right) + \gamma\frac{\beta_m^2 + \beta_e^2 + 2\alpha\gamma}{2\lambda_1 - (\beta_m + \beta_e)}\left(\frac{1}{Pe_m} - \frac{1}{Pe_e}\right)\right] \\
& + 2t_{\text{inj}}\frac{L^3}{u^3}\left[\gamma(\beta_m^2 + \beta_e^2 + \alpha\gamma + \beta_m\beta_e)\left(1 + \frac{3}{Pe_m} + \frac{3}{Pe_e} + \frac{6}{Pe_m^2} + \frac{6}{Pe_e^2}\right)\right. \\
& \left. + \gamma\frac{\beta_m^3 + \beta_e^3 + 3\alpha\gamma(\beta_m + \beta_e)}{2\lambda_1 - (\beta_m + \beta_e)}\left(\frac{3}{Pe_m} - \frac{3}{Pe_e} + \frac{6}{Pe_m^2} - \frac{6}{Pe_e^2}\right)\right] \\
& + \frac{L^4}{u^4}\left[\gamma(\beta_e^3 + 2\alpha\gamma(\beta_m + \beta_e) + \beta_m^2\beta_e + \beta_m\beta_e^2 + \beta_m^3)\left(1 + \frac{6}{Pe_m} + \frac{6}{Pe_e} + \frac{30}{Pe_m^2} + \frac{30}{Pe_e^2} + \frac{60}{Pe_m^3} + \frac{60}{Pe_e^3}\right)\right. \\
& \left. + \gamma\frac{4\beta_m\beta_e\alpha\gamma + 4\alpha\gamma(\beta_m^2 + \beta_e^2) + 2\alpha^2\gamma^2 + \beta_m^4 + \beta_e^4}{2\lambda_1 - (\beta_m + \beta_e)}\left(\frac{6}{Pe_m} - \frac{6}{Pe_e} + \frac{30}{Pe_m^2} - \frac{30}{Pe_e^2} + \frac{60}{Pe_m^3} - \frac{60}{Pe_e^3}\right)\right],
\end{aligned} \tag{A-14}$$

$$\begin{aligned}
\mu_{21}^4 =& t_{\text{inj}}^3 \frac{L}{u}\alpha + 2t_{\text{inj}}^2 \frac{L^2}{u^2}\left[\alpha(\beta_m + \beta_e)\left(1 + \frac{1}{Pe_m} + \frac{1}{Pe_e}\right) + \alpha\frac{\beta_m^2 + \beta_e^2 + 2\alpha\gamma}{2\lambda_1 - (\beta_m + \beta_e)}\left(\frac{1}{Pe_m} - \frac{1}{Pe_e}\right)\right] \\
& + 2t_{\text{inj}}\frac{L^3}{u^3}\left[\alpha(\beta_m^2 + \beta_e^2 + \alpha\gamma + \beta_m\beta_e)\left(1 + \frac{3}{Pe_m} + \frac{3}{Pe_e} + \frac{6}{Pe_m^2} + \frac{6}{Pe_e^2}\right)\right. \\
& \left. + \alpha\frac{\beta_m^3 + \beta_e^3 + 3\alpha\gamma(\beta_m + \beta_e)}{2\lambda_1 - (\beta_m + \beta_e)}\left(\frac{3}{Pe_m} - \frac{3}{Pe_e} + \frac{6}{Pe_m^2} - \frac{6}{Pe_e^2}\right)\right] \\
& + \frac{L^4}{u^4}\left[\alpha(\beta_e^3 + 2\alpha\gamma(\beta_m + \beta_e) + \beta_m^2\beta_e + \beta_m\beta_e^2 + \beta_m^3)\left(1 + \frac{6}{Pe_m} + \frac{6}{Pe_e} + \frac{30}{Pe_m^2} + \frac{30}{Pe_e^2} + \frac{60}{Pe_m^3} + \frac{60}{Pe_e^3}\right)\right. \\
& \left. + \alpha\frac{4\beta_m\beta_e\alpha\gamma + 4\alpha\gamma(\beta_m^2 + \beta_e^2) + 2\alpha^2\gamma^2 + \beta_m^4 + \beta_e^4}{2\lambda_1 - (\beta_m + \beta_e)}\left(\frac{6}{Pe_m} - \frac{6}{Pe_e} + \frac{30}{Pe_m^2} - \frac{30}{Pe_e^2} + \frac{60}{Pe_m^3} - \frac{60}{Pe_e^3}\right)\right],
\end{aligned} \tag{A-15}$$

$$\begin{aligned}
\mu_{22}^4 =& \frac{t_{\text{inj}}^4}{5} + t_{\text{inj}}^3 \frac{L}{u}\beta_e + 2t_{\text{inj}}^2 \frac{L^2}{u^2}\left[(\beta_e^2 + \alpha\gamma)\left(1 + \frac{1}{Pe_m} + \frac{1}{Pe_e}\right) + \frac{\beta_e^3 + 3\beta_e\alpha\gamma + \alpha\gamma\beta_m - \beta_e^2\beta_m}{2\lambda_1 - (\beta_m + \beta_e)}\right.
\end{aligned}$$

$$\left(\frac{1}{Pe_m}-\frac{1}{Pe_e}\right)\Bigg]+2t_{\rm inj}\frac{L^3}{u^3}\Bigg[(\beta_e^3+\alpha\gamma\beta_m+2\beta_e\alpha\gamma)\left(1+\frac{3}{Pe_m}+\frac{3}{Pe_e}+\frac{6}{Pe_m^2}+\frac{6}{Pe_e^2}\right)$$
$$+\frac{\beta_e^4-\beta_e^3\beta_m+\alpha\gamma\beta_m^2+4\beta_e^2\alpha\gamma+2\alpha^2\gamma^2+\beta_e\alpha\gamma\beta_m}{2\lambda_1-(\beta_m+\beta_e)}\left(\frac{3}{Pe_m}-\frac{3}{Pe_e}+\frac{6}{Pe_m^2}-\frac{6}{Pe_e^2}\right)\Bigg]$$
$$+\frac{L^4}{u^4}\Bigg[(\alpha^2\gamma^2+\beta_e^4+\beta_m^2\alpha\gamma+2\beta_m\alpha\beta_e\gamma+3\beta_e^2\alpha\gamma)\left(1+\frac{6}{Pe_m}+\frac{6}{Pe_e}+\frac{30}{Pe_m^2}+\frac{30}{Pe_e^2}+\frac{60}{Pe_m^3}+\frac{60}{Pe_e^3}\right)$$
$$+\frac{\beta_e^5+\beta_m^3\alpha\gamma-\beta_e^4\beta_m+5\beta_e^3\alpha\gamma+\beta_e\beta_m^2\alpha\gamma+5\beta_e\alpha^2\gamma^2+\beta_e^2\beta_m\alpha\gamma+3\alpha^2\gamma^2\beta_m}{2\lambda_1-(\beta_m+\beta_e)}$$
$$\left(\frac{6}{Pe_m}-\frac{6}{Pe_e}+\frac{30}{Pe_m^2}-\frac{30}{Pe_e^2}+\frac{60}{Pe_m^3}-\frac{60}{Pe_e^3}\right)\Bigg]. \tag{A-16}$$

Fourth central moments: The fourth central moments are calculated as

$$\mathbf{M}_4'=[\kappa]\mathbf{M}_0=\left([\mu^4]-4[\mu^1][\mu^3]+6[\mu^1]^2[\mu^2]-[\mu^1]^4\right)\mathbf{M}_0. \tag{A-17}$$

Thus, we obtain

$$\mathbf{M}_4'=\begin{pmatrix}M_{4,m}'\\ \\ M_{4,e}'\end{pmatrix}=\begin{pmatrix}\kappa_{11} & \kappa_{12}\\ \\ \kappa_{21} & \kappa_{22}\end{pmatrix}\begin{pmatrix}M_{0,m}\\ \\ M_{0,e}\end{pmatrix}, \tag{A-18}$$

where

$$\kappa_{11}=\frac{t_{\rm inj}^4}{80}+\frac{t_{\rm inj}^2}{2}\frac{L^2}{u^2}\left[(\beta_m^2+\alpha\gamma)\left(\frac{1}{Pe_m}+\frac{1}{Pe_e}\right)+\frac{\beta_m^3+3\beta_m\alpha\gamma+\alpha\gamma\beta_e-\beta_m^2\beta_e}{2\lambda_1-(\beta_m+\beta_e)}\left(\frac{1}{Pe_m}-\frac{1}{Pe_e}\right)\right]$$
$$+\frac{L^4}{u^4}\Bigg[(\alpha^2\gamma^2+\beta_m^4+\beta_e^2\alpha\gamma+2\beta_m\alpha\beta_e\gamma+3\beta_m^2\alpha\gamma)\left(\frac{6}{Pe_m^2}+\frac{6}{Pe_e^2}+\frac{60}{Pe_m^3}+\frac{60}{Pe_e^3}\right)$$
$$+\frac{\beta_m^5+\beta_e^3\alpha\gamma-\beta_m^4\beta_e+5\beta_m^3\alpha\gamma+\beta_m\beta_e^2\alpha\gamma+5\beta_m\alpha^2\gamma^2+\beta_m^2\beta_e\alpha\gamma+3\alpha^2\gamma^2\beta_e}{2\lambda_1-(\beta_m+\beta_e)}$$
$$\left(\frac{6}{Pe_m^2}-\frac{6}{Pe_e^2}+\frac{60}{Pe_m^3}-\frac{60}{Pe_e^3}\right)\Bigg], \tag{A-19}$$
$$\kappa_{12}=\frac{t_{\rm inj}^2}{2}\frac{L^2}{u^2}\left[\gamma(\beta_m+\beta_e)\left(\frac{1}{Pe_m}+\frac{1}{Pe_e}\right)+\gamma\frac{\beta_m^2+\beta_e^2+2\alpha\gamma}{2\lambda_1-(\beta_m+\beta_e)}\left(\frac{1}{Pe_m}-\frac{1}{Pe_e}\right)\right]$$
$$+\frac{L^4}{u^4}\Bigg[\gamma(\beta_e^3+2\alpha\gamma(\beta_m+\beta_e)+\beta_m^2\beta_e+\beta_m\beta_e^2+\beta_m^3)\left(\frac{6}{Pe_m^2}+\frac{6}{Pe_e^2}+\frac{60}{Pe_m^3}+\frac{60}{Pe_e^3}\right)$$
$$+\gamma\frac{4\beta_m\beta_e\alpha\gamma+4\alpha\gamma(\beta_m^2+\beta_e^2)+2\alpha^2\gamma^2+\beta_m^4+\beta_e^4}{2\lambda_1-(\beta_m+\beta_e)}\left(\frac{6}{Pe_m^2}-\frac{6}{Pe_e^2}+\frac{60}{Pe_m^3}-\frac{60}{Pe_e^3}\right)\Bigg], \tag{A-20}$$
$$\kappa_{21}=\frac{t_{\rm inj}^2}{2}\frac{L^2}{u^2}\left[\alpha(\beta_m+\beta_e)\left(\frac{1}{Pe_m}+\frac{1}{Pe_e}\right)+\alpha\frac{\beta_m^2+\beta_e^2+2\alpha\gamma}{2\lambda_1-(\beta_m+\beta_e)}\left(\frac{1}{Pe_m}-\frac{1}{Pe_e}\right)\right]$$
$$+\frac{L^4}{u^4}\Bigg[\alpha(\beta_e^3+2\alpha\gamma(\beta_m+\beta_e)+\beta_m^2\beta_e+\beta_m\beta_e^2+\beta_m^3)\left(\frac{6}{Pe_m^2}+\frac{6}{Pe_e^2}+\frac{60}{Pe_m^3}+\frac{60}{Pe_e^3}\right)$$
$$+\alpha\frac{4\beta_m\beta_e\alpha\gamma+4\alpha\gamma(\beta_m^2+\beta_e^2)+2\alpha^2\gamma^2+\beta_m^4+\beta_e^4}{2\lambda_1-(\beta_m+\beta_e)}\left(\frac{6}{Pe_m^2}-\frac{6}{Pe_e^2}+\frac{60}{Pe_m^3}-\frac{60}{Pe_e^3}\right)\Bigg], \tag{A-21}$$

$$\kappa_{22} = \frac{t_{\text{inj}}^4}{80} + \frac{t_{\text{inj}}^2}{2}\frac{L^2}{u^2}\left[(\beta_e^2+\alpha\gamma)\left(\frac{1}{Pe_m}+\frac{1}{Pe_e}\right) + \frac{\beta_e^3+3\beta_e\alpha\gamma+\alpha\gamma\beta_m-\beta_e^2\beta_m}{2\lambda_1-(\beta_m+\beta_e)}\left(\frac{1}{Pe_m}-\frac{1}{Pe_e}\right)\right]$$
$$+\frac{L^4}{u^4}\left[(\alpha^2\gamma^2+\beta_e^4+\beta_m^2\alpha\gamma+2\beta_m\alpha\beta_e\gamma+3\beta_e^2\alpha\gamma)\left(\frac{6}{Pe_m^2}+\frac{6}{Pe_e^2}+\frac{60}{Pe_m^3}+\frac{60}{Pe_e^3}\right)\right.$$
$$+\frac{\beta_e^5+\beta_m^3\alpha\gamma-\beta_e^4\beta_m+5\beta_e^3\alpha\gamma+\beta_e\beta_m^2\alpha\gamma+5\beta_e\alpha^2\gamma^2+\beta_e^2\beta_m\alpha\gamma+3\alpha^2\gamma^2\beta_m}{2\lambda_1-(\beta_m+\beta_e)}$$
$$\left.\left(\frac{6}{Pe_m^2}-\frac{6}{Pe_e^2}+\frac{60}{Pe_m^3}-\frac{60}{Pe_e^3}\right)\right]. \tag{A-22}$$

Acknowledgment: The first author is thankful to DAAD for financial support, under the "Research Stays for University Academics and Scientists" funding program (No. 57210259).

References

Brandt, A, Mann, G., Arlt, W., 1997. Temperature gradients in preparative high-performance liquid chromatography columns. Chromatogr. A, 769, 109-117.

Cerro, R.L., Smith, w., 1969. Effects of heat realse and nonlinear equilibrium on transient adsorption. Ind. Eng. Chem. Fund., 8, 796-802.

Eigenberger, G., Kolios, G., NieKen, U., 2007. Efficient reheating of a reverse-flow reformer-An experimental study. Chem. Eng. Sci., 62, 4825-4841.

Genuchten, M.Th. Van, 1981. Analytical solutions for chemical transport with simultaneous adsorption, zeroth-order production and first order decay, J. Hydrology 49, 213-233.

Glöckler, B., Dieter, H., Eigenberger, G., NieKen, U., 2006. Efficient reheating of a reverse-flow reformer-An experimental study. Chem. Eng. Sci., 62, 5638-5643.

Gritti, F., Gilar, M., Jarrell, J.A., 2016. Quasi-adiabatic vacuum-based column housing for very high-pressure liquid chromatography. J. Chromatogr. A 1456, 226-234.

Guiochon, G., 2002. Preparative liquid chromatography. J. Chromatogr. A, 965, 129-161.

Guiochon, G., Lin, B., 2003. Modeling for preparative chromatography, Academic Press.

Guiochon, G., Felinger, A., Shirazi, D.G., Katti, A.M., 2006. Fundamentals of preparative and nonlinear chromatography, 2nd ed. ELsevier Academic press, New York.

Haynes Jr., H.W., 1986. An analysis of sorption heat effects in the pulse gas chromatography diffusion experiment. AIChE J., 32, 1750-1753.

Javeed, S., Qamar, S., Seidel-Morgenstern, A., Warnecke, G., 2011. Efficient and accurate numerical simulation of nonlinear chromatographic processes. J. Comput. & Chem. Eng., 35, 2294-2305.

Javeed, S. Qamar, S., Seidel-Morgenstern, A., Warnecke, G., 2012. Parametric study of thermal effects in reactive liquid chromatography. Chem. Eng. J. 191, 426-440.

Javeed, S., Qamar, S., Ashraf, W., Warnecke, G., Seidel-Morgenstern, A., 2013. Analysis and numerical investigation of two dynamic models for liquid chromatography, Chem. Eng. Sci. 90, 17-31.

Kruglov, A., 1994. Methanol synthesis in a simulated countercurrent moving-bed adsorptive catalytic reactor. Chem. Eng. Sci., 49, 4699-4716.

Kubin, M., 1965. Beitrag zur Theorie der Chromatographie. Collect. Czech. Chem. Commun. 30, 1104-1118.

Kubin, M., 1965. Beitrag zur Theorie der Chromatographie. 11. Einfluss der Diffusion Ausserhalb und der Adsorption Innerhalb des Sorbens-Korns. Collect. Czech. Chem. Commun. 30, 2900-2907.

Kucera, E., 1965. Contribution to the theory of chromatography: Linear non-equilibrium elution chromatography. J. Chromatogr. A 19, 237-248.

Lenhoff, A.M., 1987. Significance and estimation of chromatographic parameters. J. Chromatogr. A 384, 285-299.

Miyabe, K., Guiochon, G., 2000. Influence of the modification conditions of alkyl bonded ligands on the characteristics of reversed-phase liquid chromatography. J. Chromatogr. A 903, 1-12.

Miyabe, K., Guiochon, G., 2003. Measurement of the parameters of the mass transfer kinetics in high performance liquid chromatography. J. Sep. Sci. 26, 155-173.

Miyabe, K., 2007. Surface diffusion in reversed-phase liquid chromatography using silica gel stationary phases of different C1 and C18 ligand densities. J. Chromatogr. A 1167, 161-170.

Miyabe, K., 2009. Moment analysis of chromatographic behavior in reversed-phase liquid chromatography. J. Sep. Sci. 32, 757-770.

Qamar, S., Seidel-Morgenstern, A., 2016. Extending the potential of moment analysis in chromatography, Tends Analyt. Chem., 81, 87-101, 2016.

Rice, R.G., Do, D.D., 1995. Applied mathematics and modeling for chemical engineers. Wiley-Interscience, New York.

Ruthven, D.M., 1984. Principles of adsorption and adsorption processes, Wiley-Interscience, New York.

Sainio, T., 2005. Ion-exchange resins as stationary phase in reactive chromatography. Acta Universitatis Lappeenrantaensis 218, Diss. Lappeenranta University of Technology, Finland.

Sainio, T., Kaspereit, M., Kienle, A., Seidel-Morgenstern, A., 2007. Thermal effects in reactive liquid chromatography. Chem. Eng. Sci., 62, 5674-5681.

Sainio, T., Zhang, L., Seidel-Morgenstern, A., 2011. Adiabatic operation of chromatographic fixed-bed reactors. Chem. Eng. J., 168, 861-871.

Schneider, P., Smith, J.M., 1968. Adsorption rate constants from chromatography. A.I.Ch.E. J. 14, 762-771.

Suzuki, M., 1973. Notes on determining the moments of the impulse response of the basic transformed equations. J. Chem. Eng. Japan 6, 540-543.

Vu, T.D., Seidel-Morgenstern, A., 2011. Quantifying temperature and flow rate effects

on the performance of a fixed-bed chromatographic reactor. J. Chromatogr. A, 1218, 8097-8109.

Van Deemter, J.J., Zuiderweg, F.J., A. Klinkenberg, A., 1956. Longitudinal diffusion and resistance to mass transfer as causes of nonideality in chromatography. Chemical Engineering Science 5, 271-289.

Wolff, H.-J., Radeke, K.-H, Gelbin, D., 1980. Heat and mass transfer in packed beds-IV use of weighted moments to determine axial dispersion coefficient. Chem. Eng. Sci. 34, 101-107.

Wolff, H.-J., Radeke, K.-H, Gelbin, D., 1980. Weighted moments and the pore-diffusion model. Chem. Eng. Sci. 35, 1481-1485.

Xiu, G., Li, P., Rodrigues, A.E., 2002. Sorption-enhanced reaction process with reactive regeneration. Chem. Eng. Sci., 57, 3893-3908.

Yongsunthon, I., Alpay, E., 1999. Design of periodic adsorptive reactors for the optimal integration of reaction, separation and heat exchange. Chem. Eng. Sci., 2647-2657.

Zhong, G.M., Meunier, F., 1994. Interference and heat effects: moment analysis for two-component chromatography. J. Chromatogr. A, 658, 355-360.

Table 1: Reference parameters used in case studies.

Parameters	Values
Column length	$L = 1\,cm$
Porosity	$\epsilon = 0.4$
Interstitial velocity	$u = 0.2\,cm/min$
Henry's constant	$a_{\text{ref}} = 1$
Density times heat capacity of liquid	$\rho^L c_p^L = 4\,kJ/lK$
Density times heat capacity of particle	$\rho^S c_p^S = 4\,kJ/lK$
Dispersion coefficient	$D_z = 0.002\,cm^2/min$
Heat conductivity coefficient	$\lambda_z = 0.008\,kJ\,cm^{-1}min^{-1}$
Initial concentration	$c_{\text{init}} = 0\,mol/l$
Initial temperature	$T_{\text{init}} = 300\,K$
Inlet concentration	$c_{\text{inj}} = 1\,mol/l$
Inlet temperature	$T_{\text{inj}} = 300\,K$
Reference temperature	$T_{\text{ref}} = 300\,K$
Injection time	$t_{\text{inj}} = 1\,min$

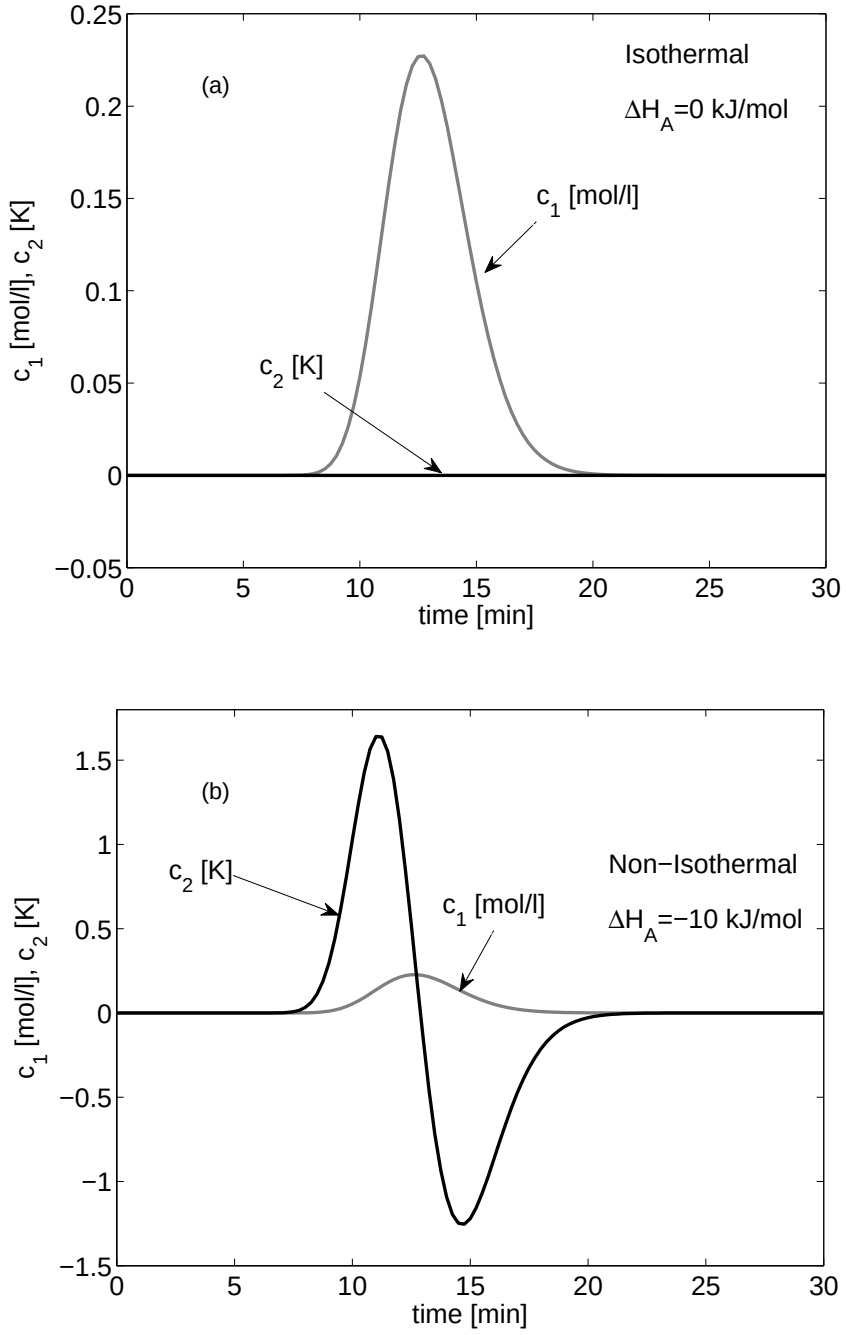

Figure 1: Effect of ΔH_A for $T_{\text{inj}} = T_{\text{init}} = 300\,K$, $\rho^S c_p^S = 4\,kJ/lk$, $\rho^L c_p^L = 4\,kJ/lk$ and $\beta_m/\beta_e = 1$.

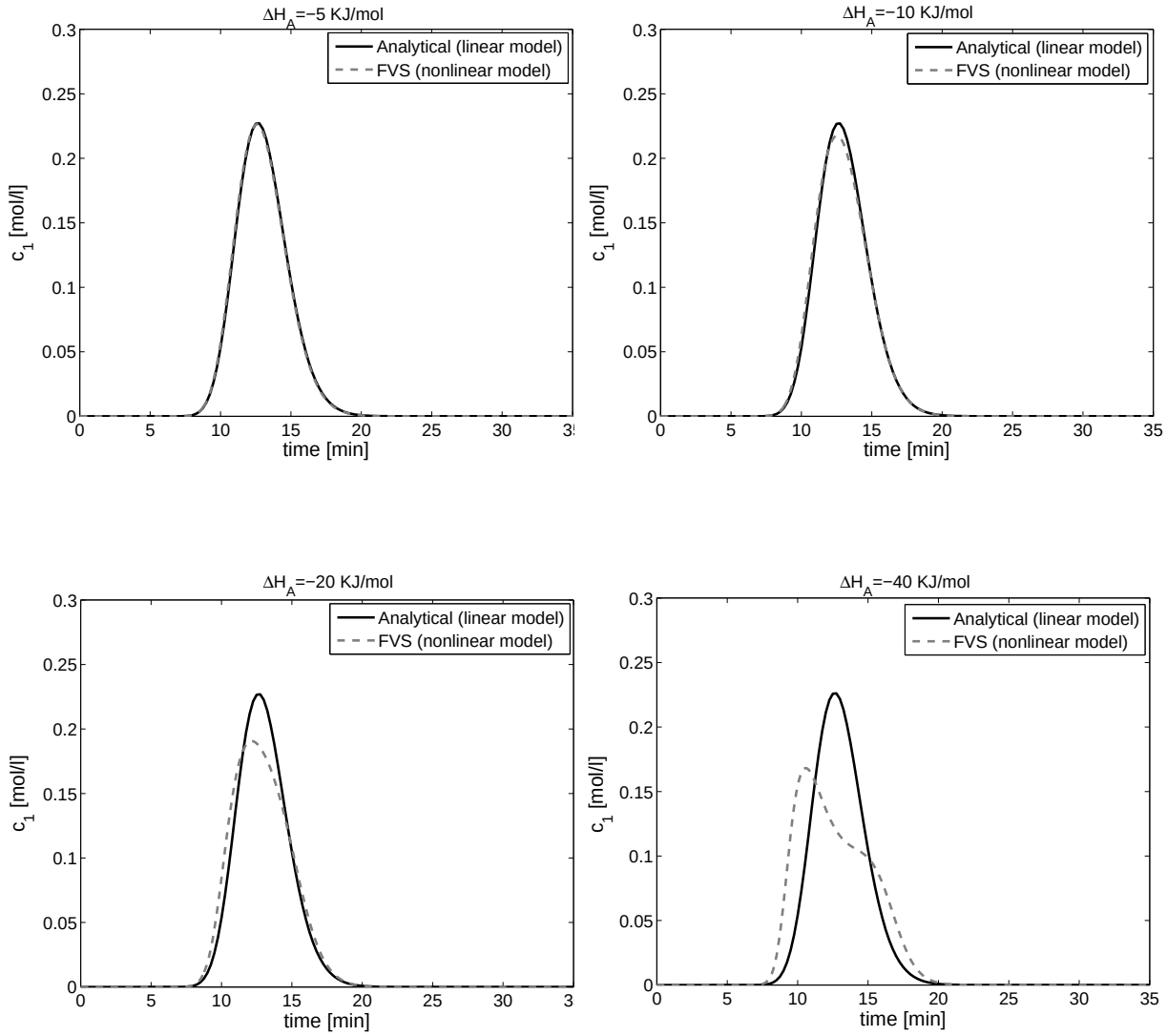

Figure 2: Comparison of analytical and numerical solutions for concentration profile at different values of enthalpy of adsorption ΔH_A. Numerical solutions are based on Eq. (3) and analytical solutions on Eq. (12). Here, $T_{\text{inj}} = T_{\text{init}} = T_{\text{ref}}$, $\rho^S c_p^S = 4\,kJ/lk$, $\rho^L c_p^L = 4\,kJ/lk$ and $\beta_m/\beta_e = 1$.

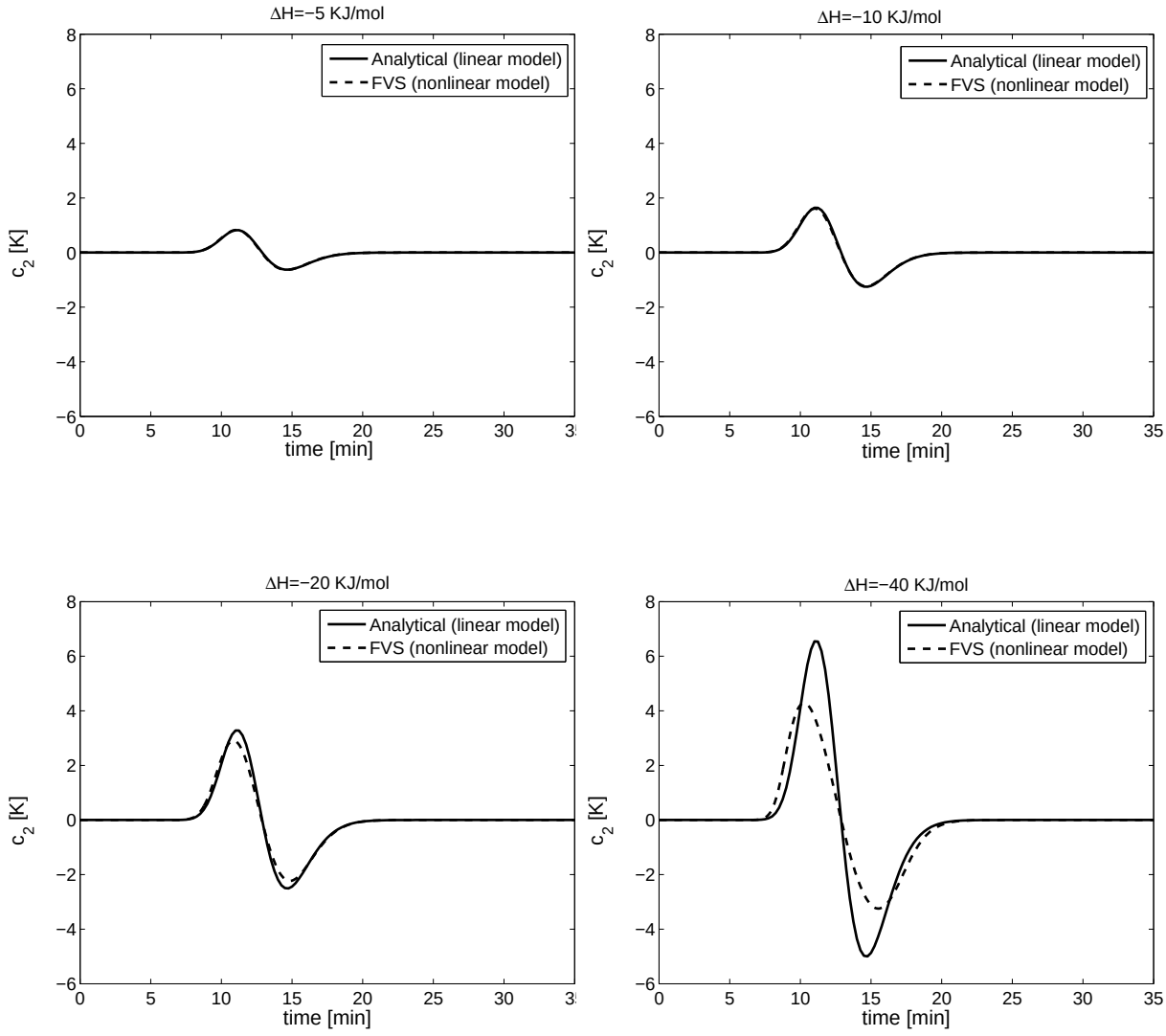

Figure 3: Comparison of analytical and numerical solutions for temperature profile at different values of enthalpy of adsorption ΔH_A. Numerical solutions are based on Eq. (3) and analytical solutions on Eq. (12). Here, $T_{\text{inj}} = T_{\text{init}} = T_{\text{ref}}$, $\rho^S c_p^S = 4\,kJ/lk$, $\rho^L c_p^L = 4\,kJ/lk$ and $\beta_m/\beta_e = 1$.

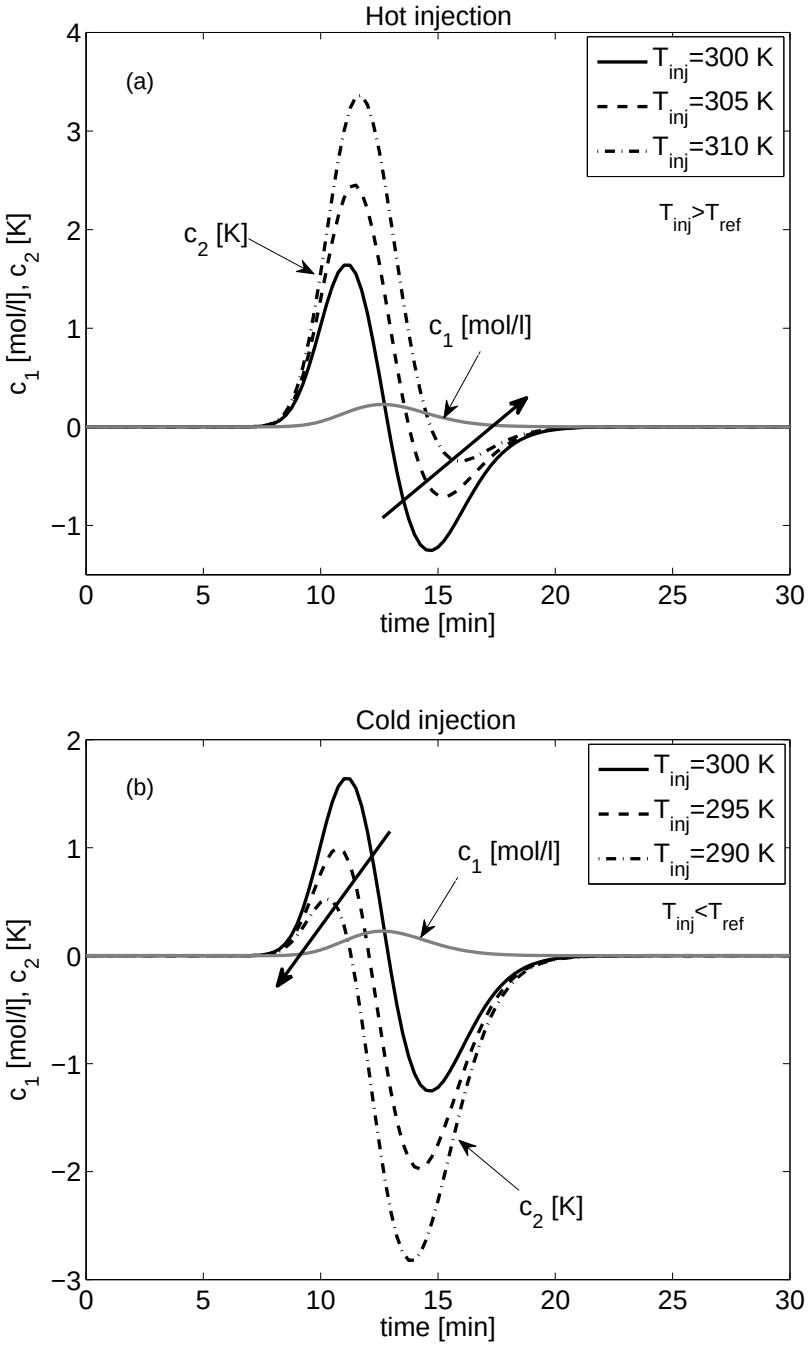

Figure 4: Effect of $T_{\text{inj}} \neq T_{\text{ref}}$ and $T_{\text{init}} = T_{\text{ref}}$ for $\Delta H_A = -10\,kJ/mol$, $\rho^S c_p^S = 4\,kJ/lk$, $\rho^L c_p^L = 4\,kJ/lk$ and $\beta_m/\beta_e = 1$.

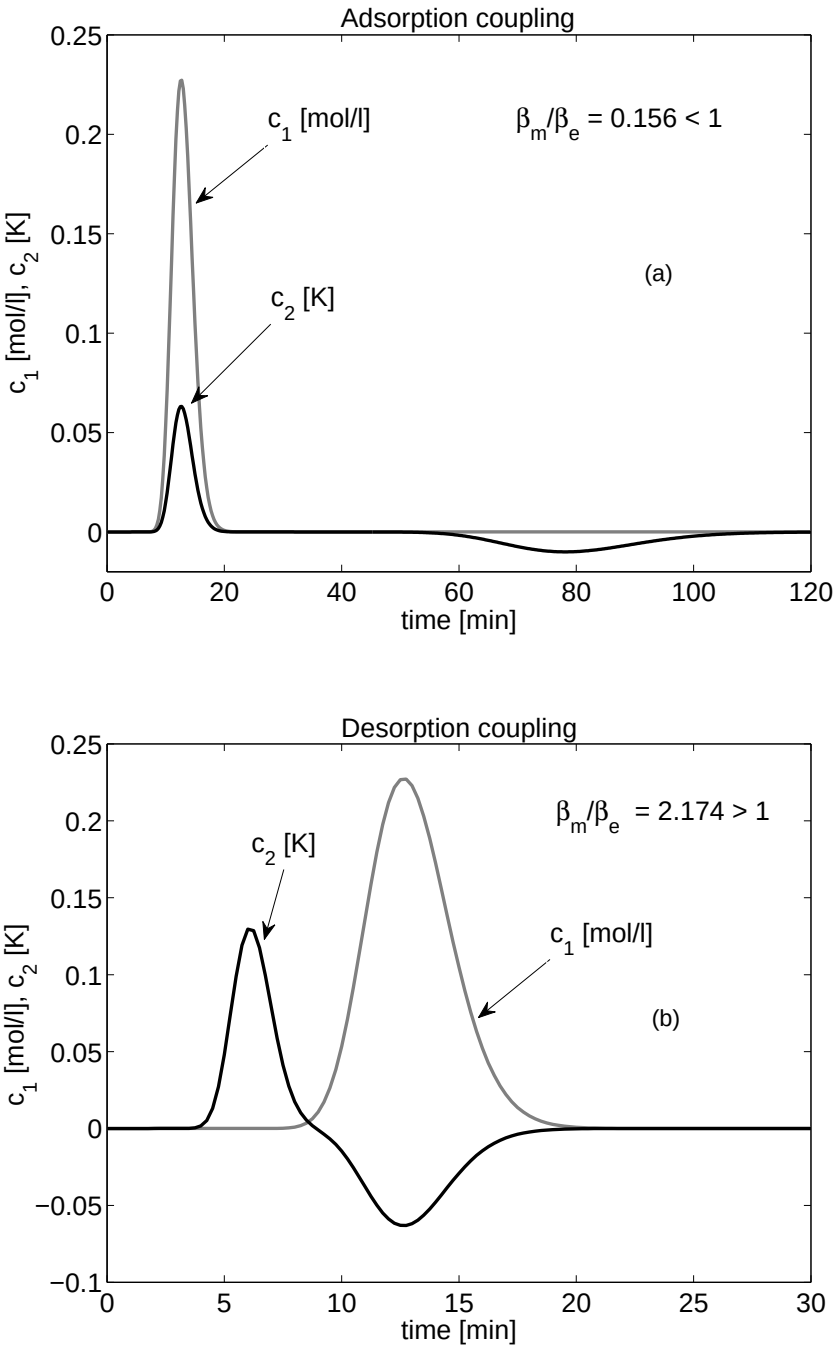

Figure 5: Effect of β_m/β_e on concentration and temperature profiles for $\Delta H_A = -10\,kJ/mol$ and $T_{\text{inj}} = T_{\text{init}} = T_{\text{ref}}$. For plot (a) $\rho^S c_p^S = 40\,kJ/lk$ and $\rho^L c_p^L = 4\,kJ/lk$, while for plot (b) $\rho^S c_p^S = 4\,kJ/lk$ and $\rho^L c_p^L = 40\,kJ/lk$.

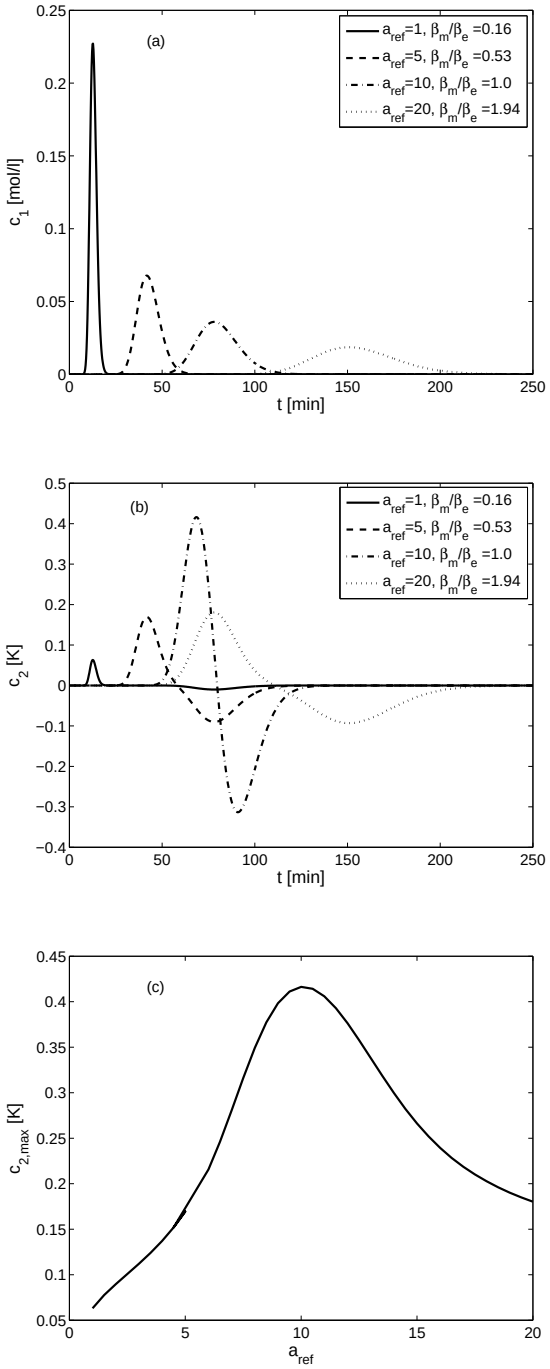

Figure 6: Plots (a) & (b): The effect of Henry's constant a_{ref} on concentration and temperature profiles. Plot (c): The maximum values of c_2 with respect to a_{ref}. Here, $\Delta H_A = -10\,kJ/mol$, $T_{\mathrm{inj}} = T_{\mathrm{init}}$, $\rho^S c_p^S = 40\,kJ/lk$ and $\rho^L c_p^L = 4\,kJ/lk$.

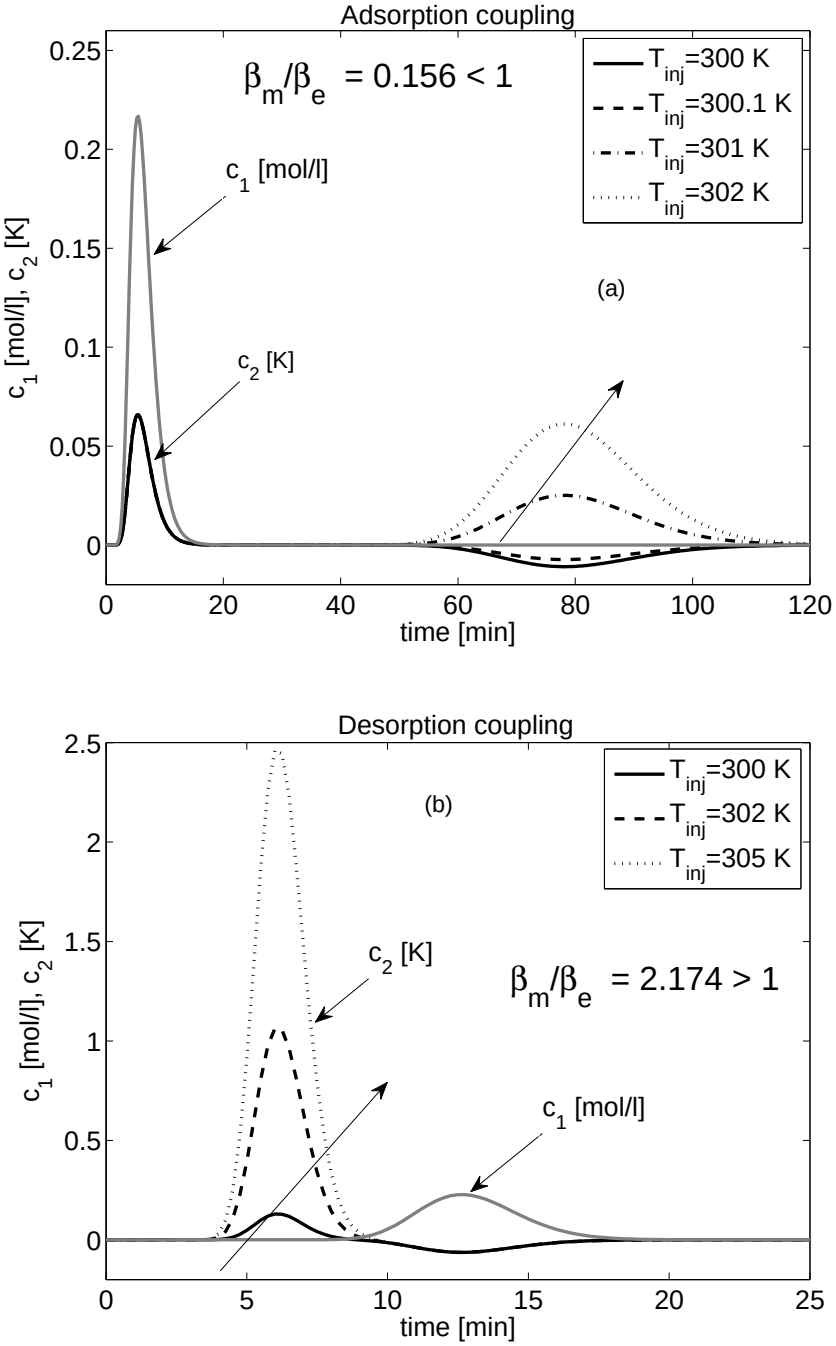

Figure 7: Effect of the $T_{\text{inj}} > T_{\text{init}}$ on concentration and temperature profiles for $\frac{\beta_m}{\beta_e} \lesseqgtr 1$ and $\Delta H_A = -10\, kJ/mol$. For plot (a): $\rho^S c_p^S = 40$ and $\rho^L c_p^L = 4$, while for plot (b): $\rho^S c_p^S = 4\, kJ/lk$ and $\rho^L c_p^L = 40\, kJ/lk$.

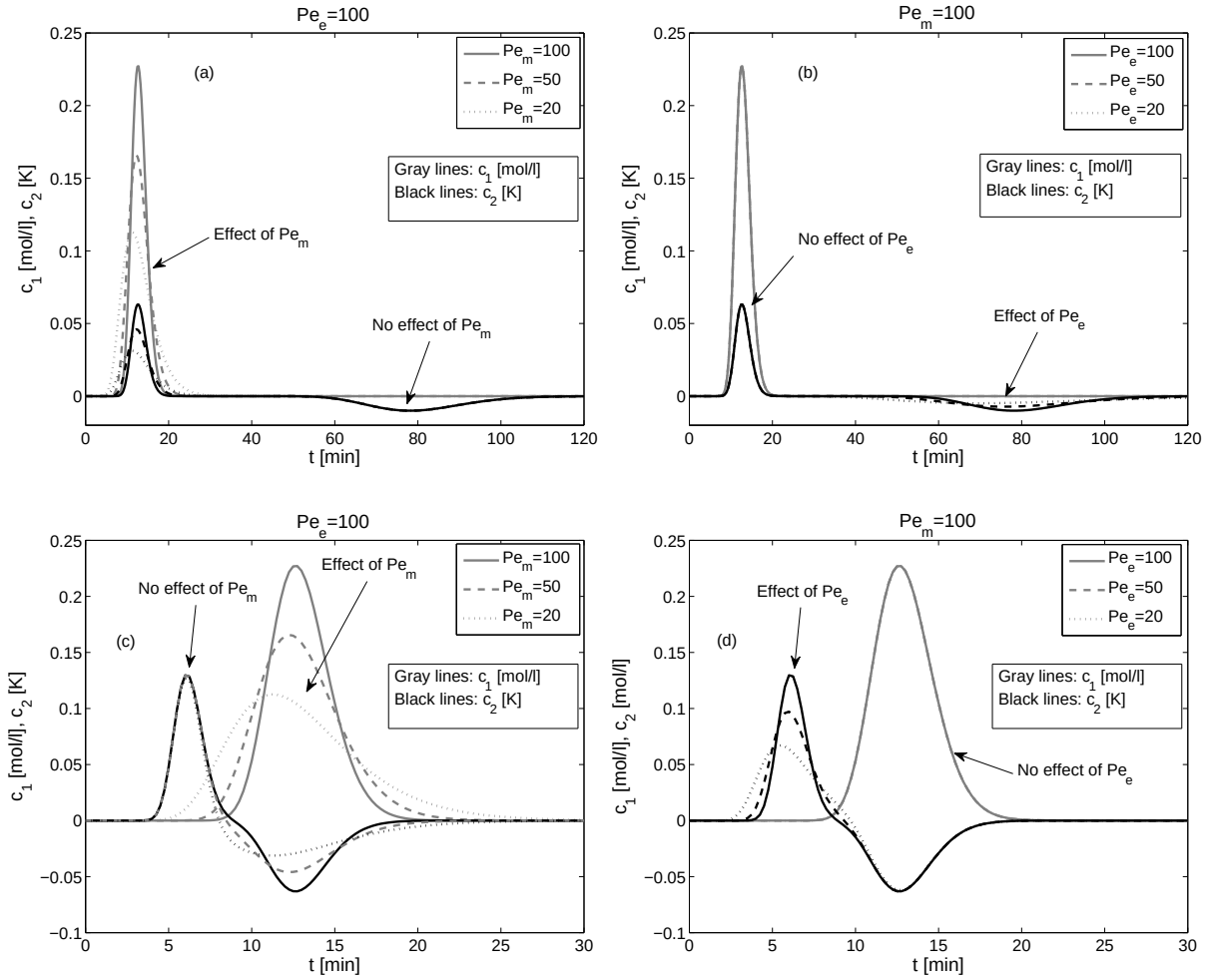

Figure 8: Effects of Peclet numbers on the concentration and temperature profiles. Here, $\frac{\beta_m}{\beta_e} = 0.156 < 1$ for cases (a) and (b), while $\frac{\beta_m}{\beta_e} = 2.174 < 1$ for cases (c) and (d). Moreover, $\Delta H_A = -10\, kJ/mol$ and $T_{\text{inj}} = T_{\text{init}} = T_{\text{ref}}$.

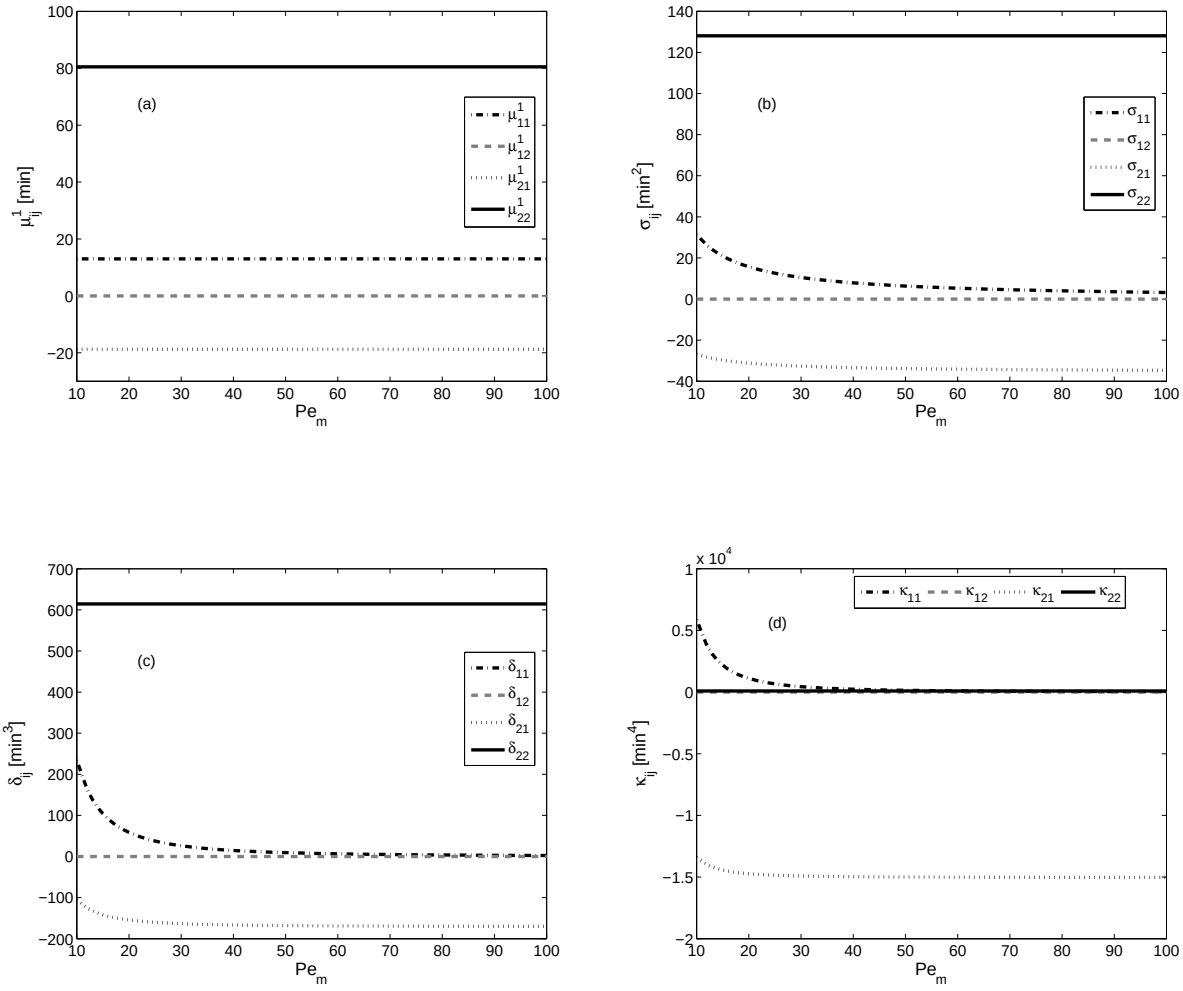

Figure 9: Effect of Pe_m on concentration and temperature moments for a fixed $Pe_e = 10^2$. Here, $\beta_m/\beta_e = 0.156 < 1$, $\rho^S c_p^S = 40\,kJ/lk$, $\rho^L c_p^L = 4\,kJ/lk$, $\Delta H_A = -10\,kJ/mol$ and $T_{\text{inj}} = T_{\text{init}} = T_{\text{ref}}$.

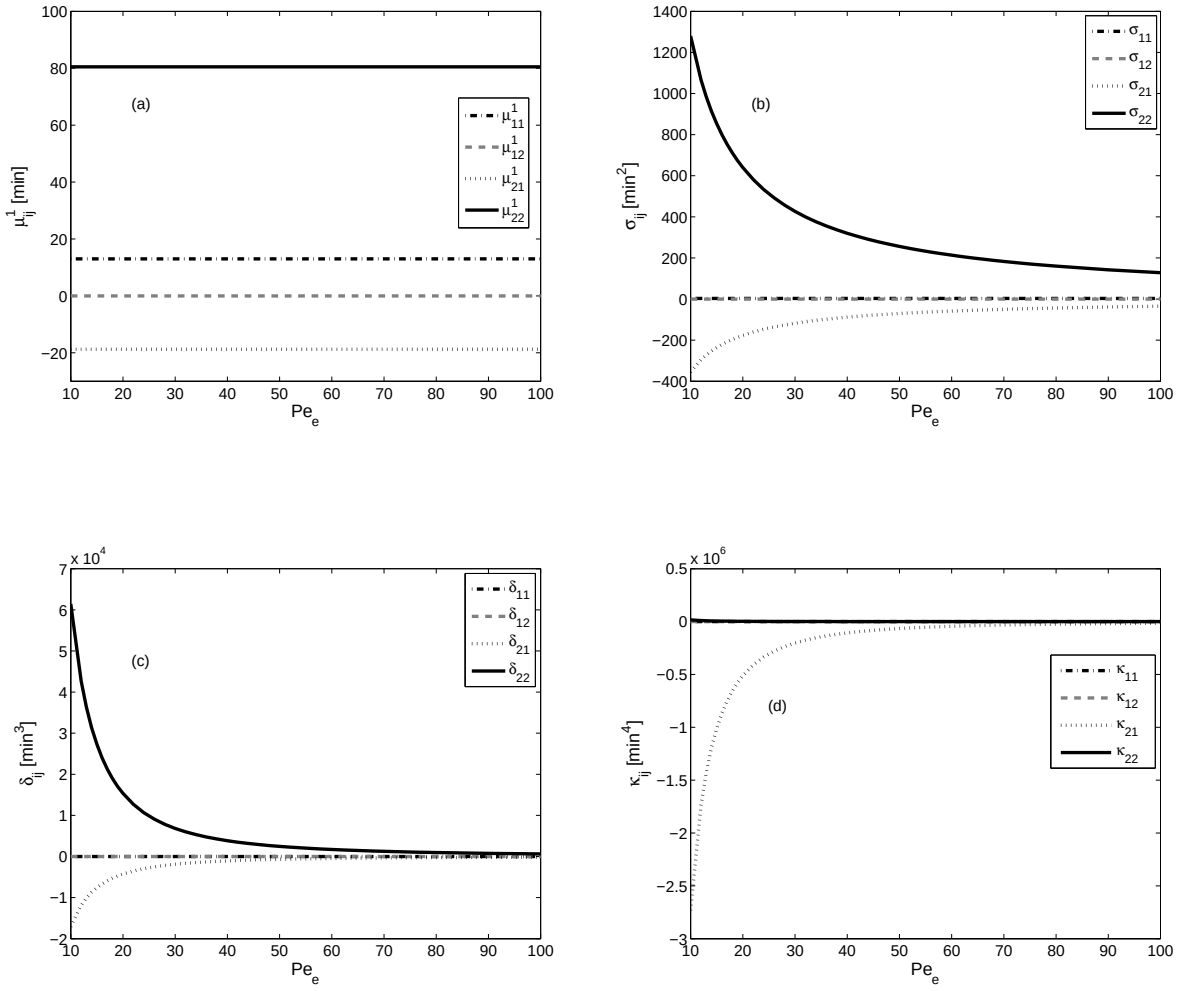

Figure 10: Effect of Pe_e on concentration and temperature moments for a fixed $Pe_m = 10^2$. Here, $\beta_m/\beta_e = 0.156 < 1$, $\rho^S c_p^S = 40\,kJ/lk$, $\rho^L c_p^L = 4\,kJ/lk$, $\Delta H_A = -10\,kJ/mol$ and $T_{\text{inj}} = T_{\text{init}} = T_{\text{ref}}$.

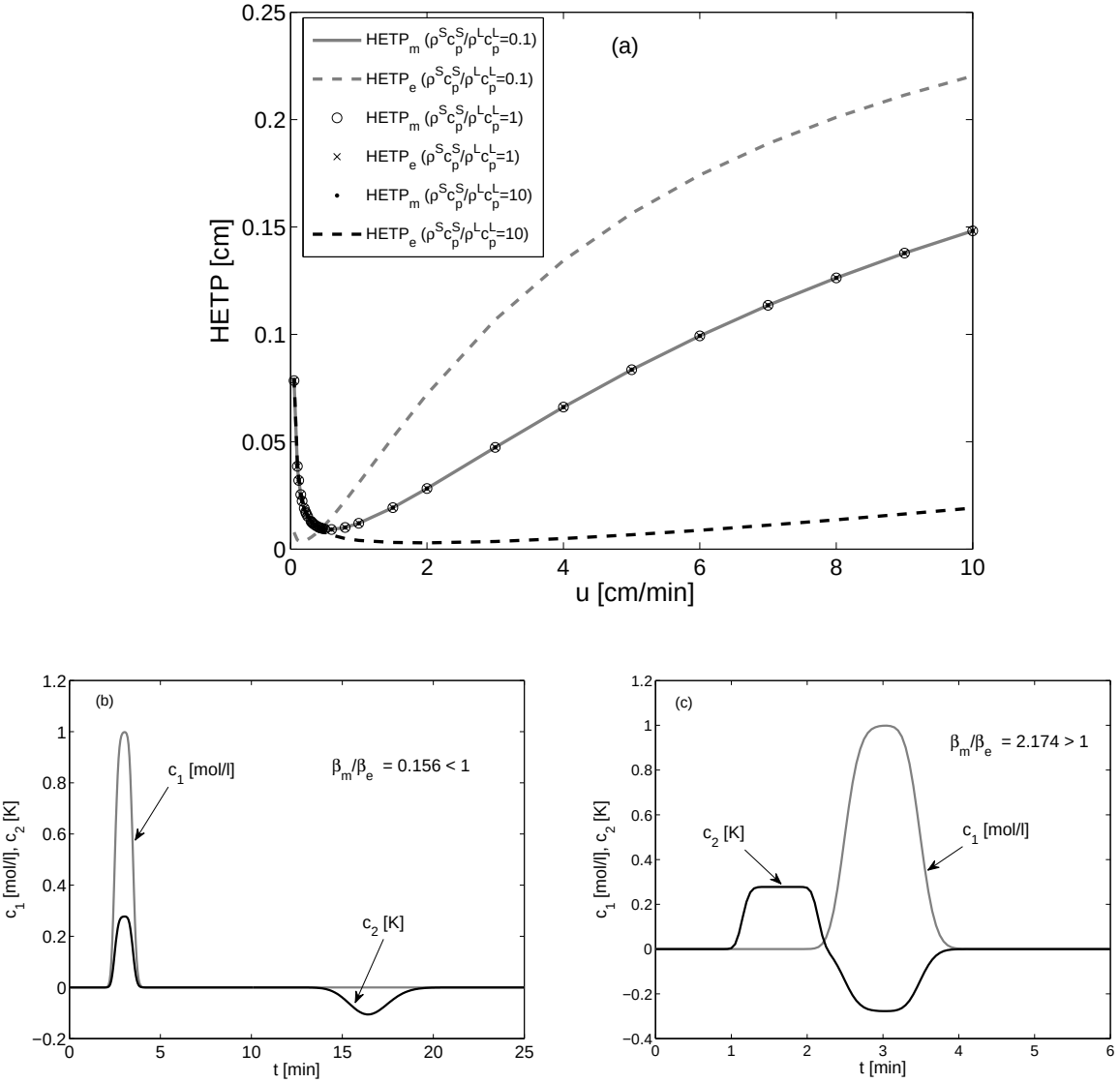

Figure 11: Top: Plots of HETP corresponding to the concentration profiles (Eq. (69)) and the temperature profiles (Eq. (70)) as functions of u. Bottom: Concentration and temperature profiles for $u = 1cm/min$ and different values of β_m/β_e. Here, $\Delta H_A = -10\,kJ/mol$, $T_{\text{inj}} = T_{\text{init}} = T_{\text{ref}}$, $D_z = 0.002\,cm^2min^{-1}$, and $\lambda_z = 0.008\,kJcm^{-1}min^{-1}$.